Available online at www.sciencedirect.com
ScienceDirect
Earth and Planetary Science Letters 255 (2007) 188–212
EPSL
www.elsevier.com/locate/epsl

Multiple sulfur isotopes from Paleoproterozoic Huronian interglacial sediments and the rise of atmospheric oxygen

Dominic Papineau [a,*,1], Stephen J. Mojzsis [a], Axel K. Schmitt [b]

[a] *Department of Geological Sciences, Center for Astrobiology, University of Colorado, Boulder, CO 80309-0399, USA*
[b] *Department of Earth and Space Sciences, University of California, Los Angeles, CA 90095-1567, USA*

Received 24 June 2006; received in revised form 27 November 2006; accepted 10 December 2006
Available online 6 February 2007
Editor: H. Elderfield

Abstract

Mass-dependently fractionated (MDF) sulfur isotopes in sedimentary sulfides and sulfates can provide information on the past activity of microbial metabolisms and serve as a proxy for the concentration of seawater sulfate. In conjunction with these proxies, mass-independently fractionated (MIF) sulfur isotopes can be used to track the rise of atmospheric oxygen. The anoxic–oxic transition of the surface environment in the Paleoproterozoic has been constrained by MIF sulfur in 2.47 Ga sulfides from Western Australian banded iron-formations, and the absence of MIF in diagenetic sulfides from 2.32 Ga black shales in the Transvaal Supergroup (South Africa). We report new multicollector ion microprobe data for individual sulfides from water-lain sedimentary units in the 2.45–2.22 Ga Huronian Supergroup (Ontario, Canada). The authigenecity of sulfides in these units is interpreted on the basis of host lithology, mode of distribution, sulfide chemistry and MDF sulfur isotopes. Sulfides interpreted to have an authigenic-sedimentary origin from the McKim Fm. have a range of 0.7‰ in $\Delta^{33}S$ values and those in the Pecors Fm. preserve small magnitude MIF $\Delta^{33}S$ values up to +0.88‰, which we propose represents the last remnants of an anoxic atmosphere. High $\delta^{34}S$ values (up to +31.2‰) and near-zero $\Delta^{33}S$ values in authigenic sulfides from the stratigraphically higher Espanola and Gordon Lake Fms. suggest local variations of seawater sulfate concentrations and/or $\delta^{34}S_{sulfate}$, consistent with increased atmospheric O_2 levels. MIF sulfur is absent from the marine record after the second Huronian glaciation, which is analogous to the record of the Transvaal Supergroup where MIF is absent from the upper part of the interglacial sequence. Our results suggest that the possible simultaneous demise of MIF sulfur isotopes at these two localities may serve as a useful global geochemical marker to correlate Paleoproterozoic supergroups. We propose a new biogeochemical model where enhanced weathering rates during Paleoproterozoic post-glacial thawing served as a critical stimulus for interglacial blooms of oxygenic photosynthesis, the demise of methane, and ultimately to the irreversible rise in atmospheric oxygen.

Keywords: Paleoproterozoic; atmospheric oxygen; sulfur isotopes; glacial–interglacial; Huronian Supergroup; ion microprobe; mass-independent fractionation

1. Introduction

Multiple lines of evidence suggest that the terrestrial atmosphere underwent a stepwise increase in oxygen content during the Paleoproterozoic [1]. The

* Corresponding author. Tel.: +1 202 478 8908; fax: +1 202 478 8901.
E-mail address: dpapineau@ciw.edu (D. Papineau).
[1] Present address: Geophysical Laboratory, Carnegie Institution of Washington, 5251 Broad Branch Road NW, Washington, DC 20015, USA.

0012-821X/$ - see front matter © 2006 Elsevier B.V. All rights reserved.
doi:10.1016/j.epsl.2006.12.015

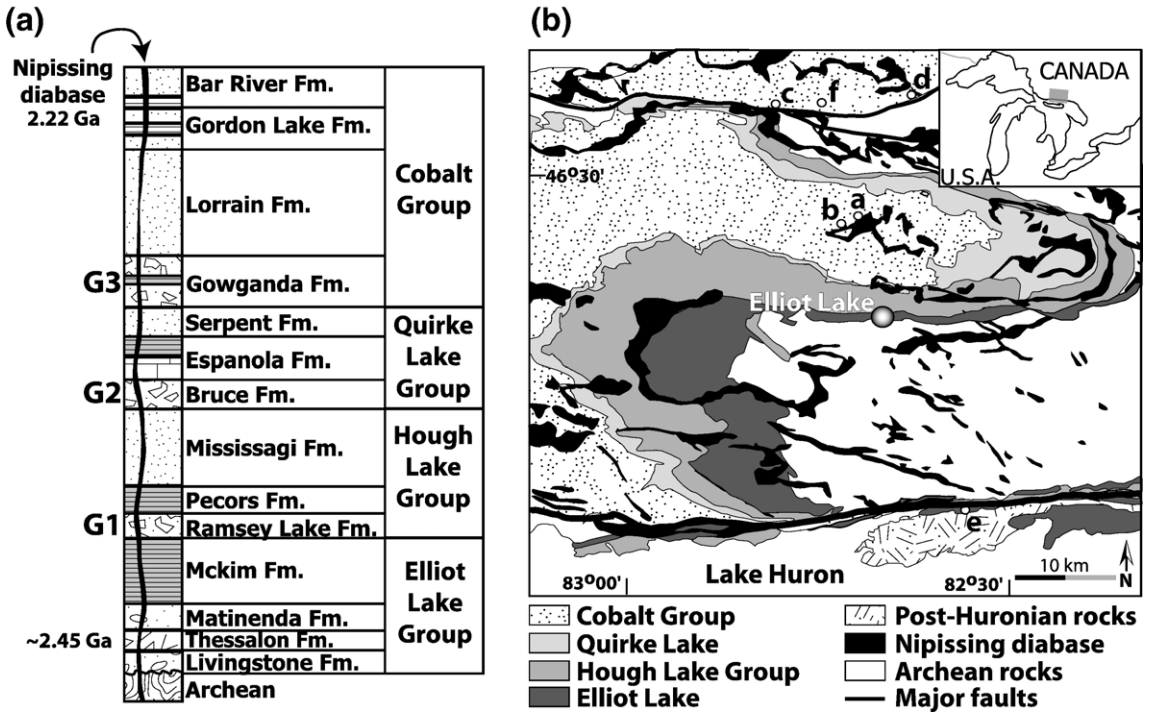

Fig. 1. (a) Idealized simplified stratigraphy of the Huronian Supergroup showing the three glacial events (labeled G1 to G3). (b) Geological map of the western portion of the Huronian Supergroup near Elliot Lake based on Ontario Geological Survey *map 2419*. Drill sites are shown for (a) core *Kerr-McGee 150-4*, (b) core *Kerr-McGee 156-1*, (c) core *Canadian Johns Manville 157-68-1* and (d) core *Sutherland and associates STAG-2*; while field sites include (e) McKim sample *HU0415* and (f) Gordon Lake sample *HU0407*.

accumulation of O_2 at that time and its effects can be traced with mass-independently fractionated (MIF) sulfur isotopes (expressed as $\Delta^{33}S$ values[2]) in sedimentary sulfide and sulfate minerals [2]. Model studies have shown that in an atmosphere essentially devoid of O_2 (<0.0002 vol.% [3]), ultraviolet photochemical reactions can produce MIF sulfur isotope signatures from SO_2 gas mixtures [4]. Archean metasedimentary rocks often preserve MIF sulfur isotopes but younger sedimentary rocks from the Proterozoic and Phanerozoic generally have mass-dependently fractionated (MDF) $\Delta^{33}S$ values close to 0.00‰ [2,5,6]. The disappearance of large magnitude MIF sulfur isotopes in the geological record is thought to have occurred sometime between 2.32 and 2.47 Ga [2,6,7]. Finely disseminated euhedral pyrite in the 2.52 Ga Gamohaan Fm. (Transvaal Supergroup, South Africa) [2,5] and pyrite bands from the 2.47 Ga Brockman Iron Fm. (Mount Bruce Supergroup, Western Australia) [2,7] preserve resolvable MIF sulfur isotopes, which stands in marked contrast with diagenetic pyrite nodules from the 2.32 Ga Timeball Hill Fm. (Transvaal Supergroup) that contain no resolvable MIF signatures [6]. Significantly, the Timeball Hill pyrite nodules stratigraphically rest between two glacially derived diamictites in the upper Timeball Hill Fm. and in the lower Duitschland Fm., which can be interpreted to indicate that significant O_2 had already begun to accumulate in the atmosphere before the end of Paleoproterozoic glaciations [6]. The range of sulfur isotope ratios recorded in sedimentary sulfide has long been used as a biosignature for the activity of microbial sulfate reduction (MSR) and as a proxy to trace the concentration of seawater sulfate (e.g. [8]). When sulfate is in non-limiting concentrations (>200 μM), MSR produces sulfide with sulfur isotope fractionations (expressed in the conventional delta notation as $\delta^{34}S$) up to 46‰, but it imparts minimal fractionation to sulfide when sulfate concentration is lower than ~200 μM [9]. Therefore large differences between $\delta^{34}S_{sulfate}$ and $\delta^{34}S_{sulfide}$ in sedimentary sulfate and sulfide minerals have been used to track the activity of

[2] $\Delta^{33}S$ (‰) = $1000 \cdot [(1+\delta^{33}S/1000) - (1+\delta^{34}S/1000^{\lambda})]$, where $\delta^{3X}S$ (‰) = $1000 \cdot [{}^{3X}S/{}^{32}S)/({}^{3X}S/{}^{32}S)_{CDT} - 1]$ and λ expresses the mass-dependent fractionation relationship between $\delta^{33}S$ and $\delta^{34}S$.

MSR, such that small differences suggest low seawater sulfate concentrations at the time of sedimentation. For instance, microscopic pyrite crystals hosted in barite from the early Archean North Pole rocks (Pilbara Craton of Western Australia) are depleted in ^{34}S with respect to ^{32}S by up to 24‰ compared to the barite matrix, which has been interpreted to indicate MSR more than 3.47 Gyr ago [10]. However such large ranges of sulfur isotope compositions are uncommon in Archean sediments, until the end of the Late Archean [8,11].

2. Geological background

2.1. Brief geological history of the Huronian Supergroup

The Huronian Supergroup is an early Paleoproterozoic volcanosedimentary succession more than 10 km thick and is best exposed immediately north of Lake Huron in Ontario, Canada. Huronian rocks are constrained in age by the basal Copper Cliff rhyolite with a zircon U–Pb age of 2.49–2.45 Ga [12] and by the Nipissing diabase that intrudes the entire supergroup with a baddeleyite U–Pb age of 2.219±0.004 Ga [13]. The Huronian Supergroup is divided by unconformities into four groups: the Elliot Lake, Hough Lake, Quirke Lake and Cobalt groups. Comparison of age constraints and lithologies for the Huronian and Snowy Pass (Wyoming, USA) supergroups highlights similarities between these rock successions, and it has been suggested that these two supergroups are contiguous [14]. These relationships, as well as volcanic activity recorded in the lower Huronian, were proposed to represent the product of a Wilson cycle with early sedimentation in an active rift basin followed by subsequent deposition in a passive plate margin setting [15,16]. The Huronian succession is punctuated by three glacial–interglacial cycles represented by diamictites (Fig. 1a). The glaciogenic origin of the Huronian diamictites is manifest by the presence of dropstones in pelitic interbeds in diamictites (G1 to G3) and of a cap carbonate above the Bruce diamictite (G2) [17,18]. Outcrops of the lower Huronian series are less widespread than those of the upper Huronian (beginning with the Gowganda Fm.), especially in the eastern part of the belt (only the western part is shown in Fig. 1b). Details of Huronian stratigraphy and tectonic history are discussed elsewhere [15,16,19,20] and a brief overview of the geology and interpretations relevant to this study is provided below.

Table 1
Brief sample description

Sample name*	Drill core or GPS coordinates	Depth (ft)	Formation	Rock type	Mineralogy†	Sulfide phase
SM0017_1634.9	KERR-McGEE 150-4	5364.0	Matinenda Fm.	Argillite	Qtz+Mi+Ilm−Fe-ox−Su	Ch+Py+Po
SM0017_1590.8	KERR-McGEE 150-4	5219.1	McKim Fm.	Argillite	Qtz+Mi−Su−Cal−Ilm−Ap−Zr	Po
SM0017_1539.6	KERR-McGEE 150-4	5051.2	McKim Fm.	Argillite	Qtz+Mi+Mu−Fe-ox−Su−An−Zr	Py
SM0017_848.0	KERR-McGEE 150-4	2782.0	Espanola Fm.	Siltstone	Mi+Qtz−Mu−Su−Ap−REEP	Py
SM0175_1542.0	KERR-McGEE 156-1	5059.1	McKim Fm.	Argillite	Qtz+Mi−Ilm−Su−Ti-ox	Po
SM0175_1420.1	KERR-McGEE 156-1	4659.0	Pecors Fm.	Argillite	Qtz+Mi+Su	Po
SM0175_1413.8	KERR-McGEE 156-1	4638.5	Pecors Fm.	Argillite	Mi+Qtz−OM−Su	Po+Sph
SM0175_1388.5	KERR-McGEE 156-1	4555.6	Pecors Fm.	Argillite	Mi+Qtz−OM−Su	Py
SM0175_1383.5	KERR-McGEE 156-1	4539.0	Pecors Fm.	Argillite	Mi+Qtz−Su	Py+Po
SM0175_1375.4	KERR-McGEE 156-1	4512.5	Pecors Fm.	Argillite	Mi+Qtz−Ti-ox−Su− Ap	Po+Ch
SM0175_1368.1	KERR-McGEE 156-1	4488.5	Pecors Fm.	Argillite	Mi+Qtz+Su−Fe-ox−Cal−An−Ap	Po
SM0175_861.4	KERR-McGEE 156-1	2826.0	Espanola Fm.	Limestone	Dol−Cal−Su−Qtz	Py
SM0175_855.9	KERR-McGEE 156-1	2808.1	Espanola Fm.	Limestone	Dol+Qtz−Cal−Mi−Su−Ap	Py
SM0175_851.2	KERR-McGEE 156-1	2792.6	Espanola Fm.	Limestone	Dol−Qtz−Su	Py
SM0175_839.6	KERR-McGEE 156-1	2754.5	Espanola Fm.	Limestone	Dol+Mu+Qtz−Su	Py+Ch
SM0175_819.2	KERR-McGEE 156-1	2687.7	Nipissing diabase	Gabbro	Cpx+Pl+Ilm−Su−Zr−Qtz	Py
SM0060_261.2	Sutherland & associates STAG-2	857.0	Gordon Lake Fm.	Argillite	Qtz+Mi− Su−Mu	Py
SM0406_635.8	Canadian Johns Manville 157-68-1	2086.1	Lorrain Fm.	Argillite	Qtz+Mi−Su−Fe-ox	Py
HU0415	N46°12′42.1″ W82°34′13.0″	–	McKim Fm.	Metapelite	Qtz+Bi+Mu+St−Su−Ap−REEP	Po+Ch
HU0407	N46°36′29.3″ W82°47′17.7″	–	Gordon Lake Fm.	Argillite	Qtz+Mi+Su+REEP	Py

*Sample names begin with the Sault Sainte-Marie core number followed by the depth in meters (calculated).
†Mineral abbreviations: An=anhydrite, Ap=apatite, Bi=biotite, Cal=calcite, Ch=chalcopyrite, Cpx=clinopyroxene, Dol=dolomite, Fe-ox=iron-oxide, Ilm=ilmenite, Mi=microcrystalline mica, Mu=Muscovite, OM=organic matter, Pl=Plagioclase, Po=pyrrhotite, Py=pyrite, Qtz=quartz, REEP=rare earth element phosphate, Sph=sphalerite, St=staurolite, Su=sulfides, Ti-ox=titanium-oxide, Zr=zircon. The + and − separators are for major/minor and accessory phases, respectively.

Table 2
Wavelength dispersive spectroscopic analyses of targeted sulfides (in %)

Analyzed sulfides*	Fe	S	Co	Ni	Cu	Zn	Total	Phase
SM0017_1634.9a	62.60	35.49	0.09	0.04	0.05	0	98.27	Po
SM0017_1634.9b	61.99	35.13	0.05	0	0.05	0.01	97.23	Po
SM0017_1634.9c	45.15	53.13	0.15	1.93	0.07	0	100.42	Py
SM0017_1634.9d	44.93	53.35	0.22	2.02	0.08	0.014	100.62	Py
SM0017_1590.8a	62.02	36.59	0.08	0	0.08	0.03	98.79	Po
SM0017_1590.8b	61.80	35.40	0.05	0	0.03	0.02	97.29	Po
SM0017_1590.8d	61.06	35.48	0.02	0.05	0	0	96.62	Po
SM0017_1539.6a	40.48	54.31	0.04	5.40	0.01	0	100.25	Py
SM0017_1539.6b	45.39	53.10	0.07	0.70	0.39	0.01	99.66	Py
SM0017_1539.6c	44.48	54.48	0.09	1.83	0.02	0.02	100.92	Py
SM0017_1539.6d	39.74	47.16	0.73	0.79	0.06	0.01	88.49	Py
SM0017_848.0a	46.85	54.45	0.03	0	0	0	101.33	Py
SM0017_848.0b	46.44	54.30	0.24	0	0	0	100.98	Py
SM0017_848.0c	45.16	54.05	1.95	0	0.01	0	101.17	Py
SM0017_848.0d	46.75	53.67	0.07	0.02	0.04	0.02	100.55	Py
SM0175_1542.0c	62.07	37.25	0.09	0	0	0.05	99.47	Po
SM0175_1542.0d	62.03	37.28	0.05	0.03	0.04	0	99.43	Po
SM0175_1420.1a	61.17	39.71	0.10	0.38	0	0	101.37	Po
SM0175_1420.1b	60.39	39.87	0.07	0.36	0	0	100.68	Po
SM0175_1420.1c	60.92	39.76	0.09	0.36	0	0	101.13	Po
SM0175_1413.8a	61.10	39.90	0.14	0.45	0.06	0	101.65	Po
SM0175_1413.8d	59.39	39.13	0.09	0.31	0.01	0.01	98.94	Po
SM0175_1413.8e	57.83	39.07	0.09	0.29	0.02	0.01	97.31	Po
SM0175_1388.5a	47.03	55.55	0.06	0.64	0.01	0.02	103.31	Py
SM0175_1388.5b	46.61	54.83	0.37	1.17	0	0.04	103.02	Py
SM0175_1388.5c	47.34	54.55	0.15	0.43	0	0	102.47	Py
SM0175_1383.5a	59.55	39.82	0.13	0.43	0	0.02	99.93	Po
SM0175_1383.5b	43.93	55.74	0.27	2.32	0	0	102.26	Py
SM0175_1383.5c	60.72	39.75	0.07	0.38	0.05	0.01	101.00	Po
SM0175_1375.4d1	57.93	39.24	0.12	0.44	0.01	0	97.74	Po
SM0175_1375.4d2	56.01	39.14	0.09	0.23	0.02	0.01	95.50	Po
SM0175_1375.4e	57.34	39.37	0.10	0.18	0	0	96.99	Po
SM0175_1375.4f	29.69	34.89	0.03	0	34.17	0.07	98.85	Ch
SM0175_1368.1a	58.82	39.03	0.09	0.42	0.02	0	98.39	Po
SM0175_1368.1b	57.35	39.83	0.11	0.38	0.35	0	98.02	Po
SM0175_1368.1c	58.40	39.28	0.20	0.38	0.06	0.02	98.33	Po
SM0175_861.4a	47.45	55.09	0.28	0.03	0	0	102.85	Py
SM0175_861.4b	48.09	55.25	0.19	0	0	0	103.54	Py
SM0175_855.9a	47.11	54.52	0.15	0.06	0	0	101.83	Py
SM0175_855.9b	47.26	54.49	0.53	0.04	0.03	0	102.36	Py
SM0175_855.9d	47.12	54.30	0.26	0.01	0	0.01	101.69	Py
SM0175_851.2a	47.05	54.87	0.06	0.01	0.01	0	102.00	Py
SM0175_839.6a	46.16	54.13	0.43	0.08	0.01	0.04	100.86	Py
SM0175_839.6d	46.54	54.41	0.33	0.02	0	0.01	101.31	Py
SM0175_839.6e	42.47	51.78	2.86	0	0	0.02	97.14	Py
SM0175_839.6f	44.05	53.53	2.23	0.05	0.07	0	99.93	Py
SM0175_819.2a	45.85	53.65	1.09	0	0.01	0	100.60	Py
SM0175_819.2b	46.93	53.91	0.42	0.19	0.05	0	101.50	Py
SM0175_819.2c	46.04	54.38	1.52	0	0	0	101.95	Py
SM0060_261.2a	45.86	53.39	0.03	0.01	0.03	0.05	99.37	Py
SM0060_261.2b	46.35	53.91	0.24	0.09	0.01	0	100.60	Py
SM0060_261.2c	46.24	54.51	0.38	0	0.02	0.08	101.23	Py
SM0060_261.2d	46.06	54.07	0.07	0.02	0.07	0.01	100.30	Py
SM0406_635.8a	47.07	54.37	0.07	0	0.03	0.04	101.59	Py
SM0406_635.8b	46.74	54.32	0.12	0.01	0.01	0.04	101.24	Py
SM0406_635.8c	47.10	54.60	0.02	0.03	0.06	0.03	101.84	Py
SM0406_635.8d	47.29	54.61	0.01	0.05	0	0	101.96	Py

(continued on next page)

Table 2 (*continued*)

Analyzed sulfides*	Fe	S	Co	Ni	Cu	Zn	Total	Phase
SM0406_635.8e	47.48	54.80	0.08	0.02	0.01	0.01	102.38	Py
HU0415a	58.12	40.43	0.24	0.07	0.03	0	98.89	Po
HU0415b	58.51	40.54	0.19	0.06	0	0.01	99.31	Po
HU0415c	58.59	39.66	0.05	0.51	0.07	0.01	98.89	Po
HU0415d	29.90	35.91	0	0	36.47	0.06	102.34	Ch
HU0415e	29.93	35.94	0.05	0	35.84	0.03	101.79	Ch
HU0407a	46.19	51.75	0.06	0.06	0.01	0	98.08	Py
HU0407b	45.58	52.75	0.17	0.17	0.07	0	98.74	Py
HU0407c	46.29	52.03	0.04	0	0.03	0	98.39	Py
HU0407d	46.09	52.49	0.10	0.07	0.02	0.01	98.77	Py

*Nomenclature for the analyzed sulfides is the sample name (core name followed by depth in meters or HU04 followed by sample number) followed by a letter for specific sulfide grains in the thin section. As a general rule, the WDS data presented are reliable to approximately 100 ppm depending on the element.

The lowermost Huronian rocks of the Livingstone Creek Fm. are primarily composed of arkosic sandstones with minor conglomerate and fine-grained siltstones [14,15]. These detrital sediments rest unconformably on the Archean basement and their geochemical characteristics indicate deposition as paleosols, likely due to the initiation of rifting in the Huronian [15,21]. The presence of tholeiites and volcaniclastic rocks in the Thessalon Fm. is consistent with an early period of rifting in the basin [14,15]. The overlying conglomerates and sandstones of the Matinenda Fm. are known to host detrital uraninite placers [18] as well as kerogen of biological origin (possibly from cyanobacteria) based on interpretations of organic biomarkers and carbon isotopes [22–24]. Interbedded sandstones and conglomerates in the Matinenda Fm. point to variations the bedload capacity of fluvial inputs to the basin until deposition of the McKim Fm. [25]. A succession of sandstones, siltstones, argillites and mudstones compose the McKim Fm. and this gradual facies change from fluvial to clay-rich sediments has been proposed to indicate a transgressive deltaic sequence [25]. It is not clear whether the depositional environment of the upper parts of the McKim Fm. was deep lacustrine or marine (e.g. [15,25]). The ensuing Ramsey Lake diamictite, which contains dropstones in siltstone interbeds, implies deposition in a glaciomarine setting at an ice margin. These glacially-derived sediments are followed by the Pecors Fm. with siltstones and finely laminated argillites perhaps deposited in a lacustrine or restricted rift basin. The Pecors Fm. has been interpreted to record deposition as a pro- to distal deltaic environment that preceded the formation of the Mississagi delta [15,25]. Sandstones and arkoses of the Mississagi Fm. are succeeded by the glacially derived Bruce Fm., which contains dropstones [26] and is immediately overlain by a carbonate with carbon isotope characteristics that broadly resemble those described for Neoproterozoic cap carbonates [17]. Sedimentary rocks of the post-glacial Espanola Fm. constitute a transition from a lower carbonate–limestone member to a higher siltstone-heterolithic member, which is interpreted to have formed in a shallow-marine or restricted lacustrine environment possibly during a period of active continental fragmentation [15,27–29]. Rare columnar stromatolite features have also been reported in the Espanola carbonate [30]. During subsequent marine regression, siliciclastic sedimentation in the Serpent Fm. occurred under alluvial or fluvial conditions during rifting. Climate cooling and deposition in a passive margin typify the upper Huronian rocks [15].

Upper Huronian rocks of the Cobalt Group contain the oldest red beds of the Huronian succession, and have attributes that indicate deposition on a continental shelf during a final period of rifting and regional subsidence [15,31]. Slump movements and faulting were coincidental with the deposition of the Gowganda glaciomarine sequence of diamictites and dropstone-containing argillites and mudstones [16]. The Lorrain Fm. conformably overlies the Gowganda Fm. and is primarily composed of arkosic and aluminous sandstones, varicolored siltstones and conglomerates interpreted to have deposited under shallow-marine, alluvial and/or fluvial conditions [32,33]. Unfortunately, studies of remanent magnetization in the Gowganda and Lorrain formations have not unambiguously provided estimates of the paleolatitude of the Upper Huronian [34,35]. The Gordon Lake Fm. consists of mudstones, siltstones, cherts and sandstones that deposited in tidally influenced shallow-marine conditions on the passive margin [15,36]. Gypsum and jasper nodules in the Gordon Lake Fm. suggest more oxidizing conditions during sedimentation in a sabkha-type environment [37]. The post-depositional history of Huronian rocks included ~2.2 Ga metamorphism associated with the

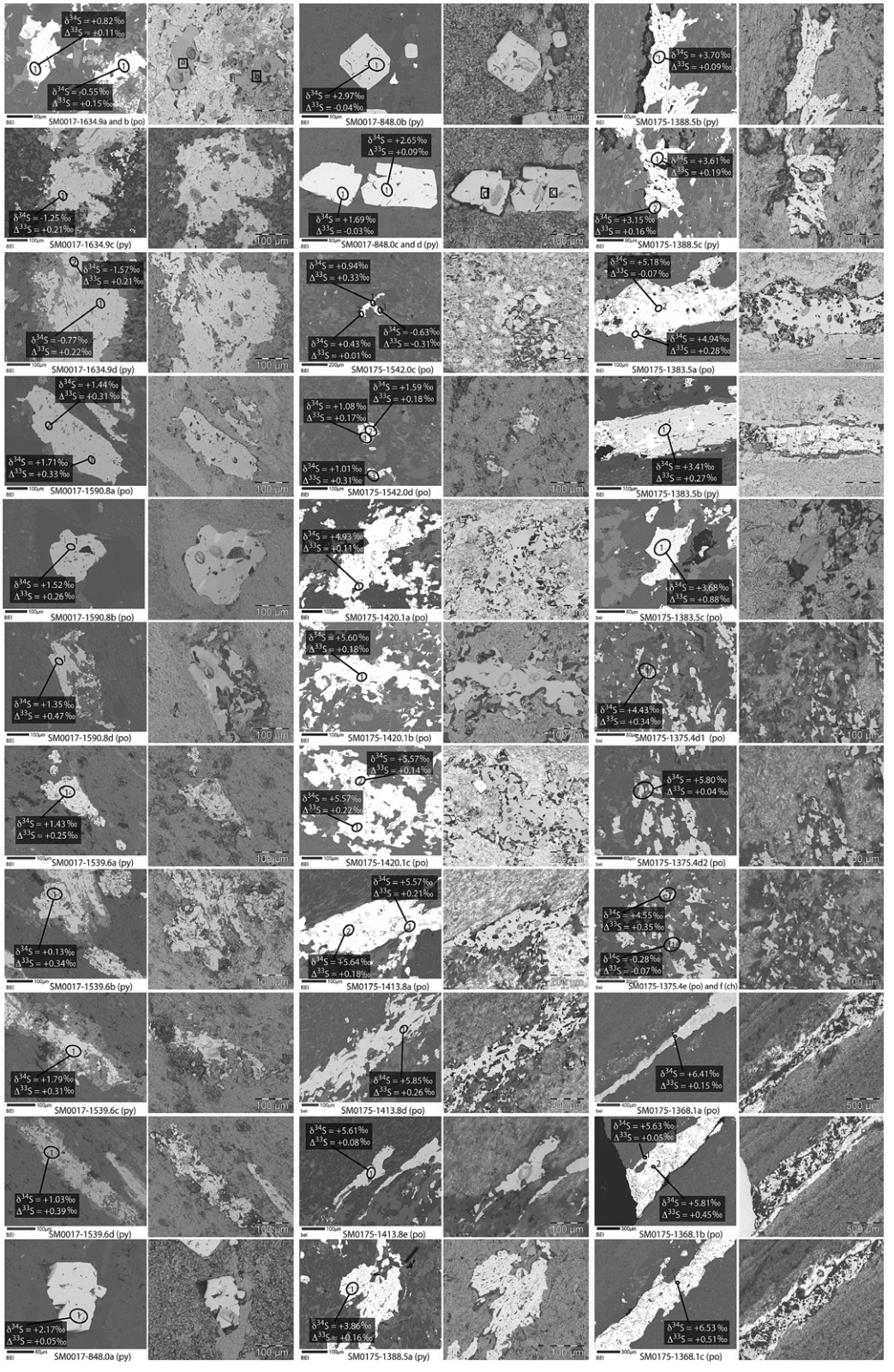

Fig. 2. Three columns of paired backscattered electron (BSE — left) and transmitted/reflected light (TL/RL — right) images of all analyzed target sulfides. Ion microprobe spots in the TL/RL images without sulfur isotope ratios were test spots for aiming and focusing the primary Cs^+ beam.

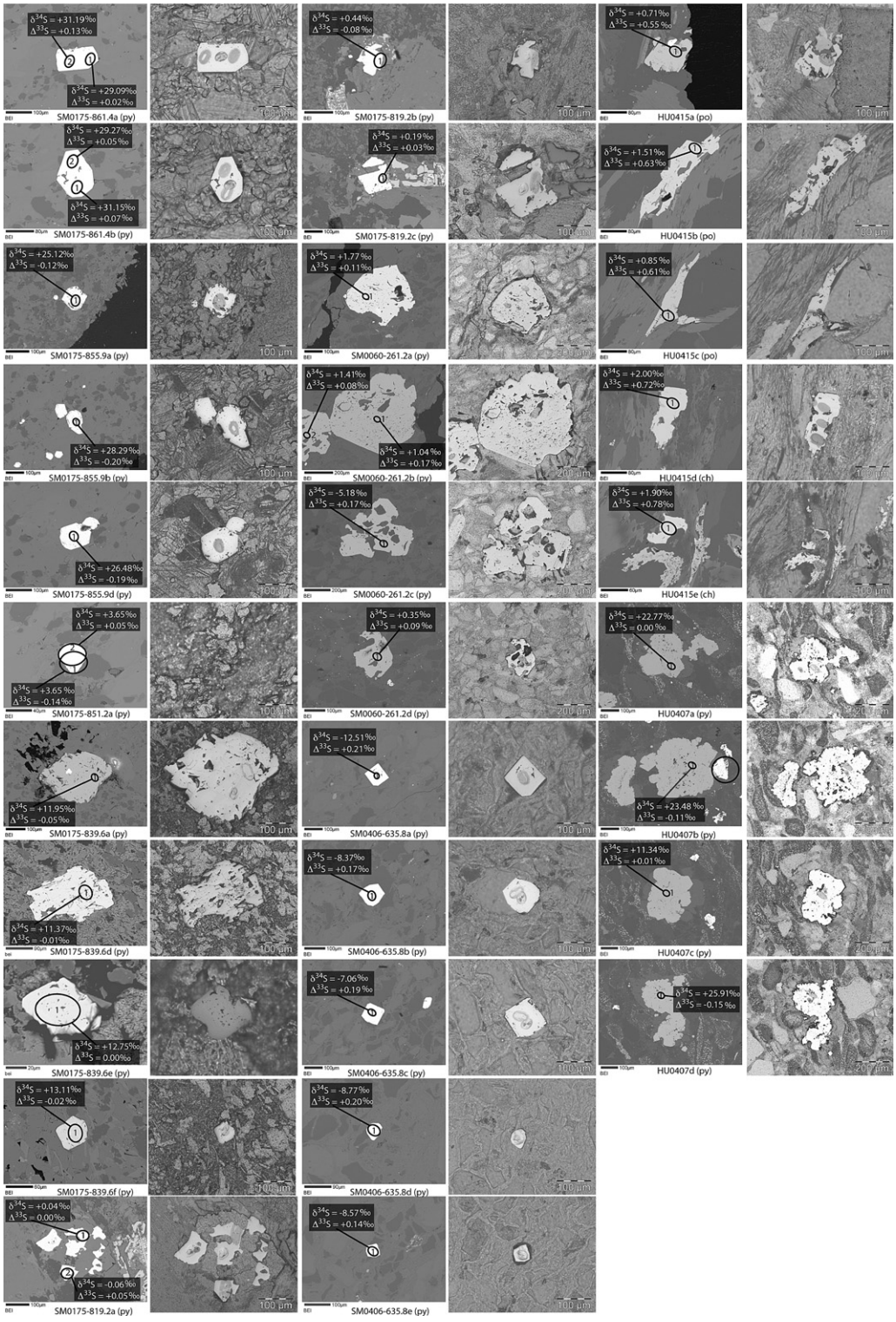

Fig. 2 (*continued*).

emplacement of the Nipissing diabase [13], a major metamorphic event at ~1.85 Ga with the culmination of the Penokean Orogeny [19] and alkaline metasomatism around 1.7 Ga [38]. Metamorphic grades in Huronian rocks are generally sub-greenschist to greenschist facies, but they also exist at amphibolite grade near the Murray tectonic fault zone (Fig. 1b).

2.2. Redox changes in the Huronian Supergroup

Sedimentary rocks of the Huronian Supergroup represent important vestiges of the early Paleoproterozoic because they preserve evidence for three cyclic glaciations and for the profound changes in surface redox conditions at that time. The lower Huronian Elliot Lake Group contains placers of detrital uraninite that suggest a generally anoxic atmosphere at the time of deposition, which stands in marked contrast with hematitic red beds and sandstones in the upper Huronian Cobalt Group [18]. The chemistry of lower Huronian paleosols suggests subaerial weathering under generally anoxic conditions, which is distinct from the oxidized nature of upper Huronian sediments [21]. Changes in oxidation state are also hinted at by the presence of bedded jasper-chert and primary anhydrite precipitates in the Gordon Lake Fm. [37]. The sulfur isotope composition of these anhydrite nodules has revealed $\delta^{34}S$ values between +12.3 and +15.6‰, which was interpreted to reflect the influence of fractionation possibly by MSR on $\delta^{34}S_{sulfate}$ in contemporary seawater [39]. Profound changes in the sulfur cycle are further suggested by the increased range of $\delta^{34}S$ in bulk sulfides from sediments above the third glacial diamictite [40]. Hence, the Huronian Supergroup represents an ideal proving ground for studies of multiple sulfur isotopes to trace atmospheric oxygenation. Despite geologic evidence for anoxic conditions during the deposition of the lower Huronian, MIF sulfur isotope signatures for these rocks have so far gone undetected [2,41,42]. Here we report in-situ sulfur isotope measurements on sulfides by high resolution ion microprobe from selected key sections of water-lain sediments that cover the entire Huronian Supergroup. The results allow us to (1) trace the Paleoproterozoic rise of atmospheric O_2 within a continuous rock-sequence and (2) monitor fluctuations in seawater sulfate concentrations and/or in the activity of MSR during interglacial periods.

3. Samples and methods

Samples collected from drill cores (Fig. 1b) were selected in the attempt to explore for a chemostratigraphic record of sulfur isotopes above and below the Huronian glacial diamictites. Because the authigenecity of sulfides is critical for this study, sample collection was specifically directed towards water-lain fine grained sedimentary rocks such as argillites, siltstones and limestones with sulfide occurrences. The two samples from field sites were an amphibolite-grade pelite from the McKim Fm. collected immediately north of the Murray fault and a cherty red bed from the Gordon Lake Fm. collected from a road cut. A few sulfides of detrital origin were analyzed in an attempt to assess their possible provenance. While most analyses were made on sulfides from metasedimentary rocks, four magmatic sulfides from the igneous Nipissing diabase were also analyzed for comparison. Preliminary identification of sulfides was performed by standard petrographic analyses of thin sections. Selected samples are briefly described in Table 1 and were mapped in transmitted and reflected light prior to electron probe microanalysis. Wavelength Dispersive Spectroscopic (WDS) analyses on selected target sulfides were performed to unambiguously determine the phase and to quantify trace metals (e.g. Co, Zn and Ni).

Distinction between authigenic-sedimentary sulfides and detrital or hydrothermal sulfides was based on sulfide chemistry, host lithology, mode of occurrence and isotopic composition. For instance, sulfides with unusual concentrations of Co, Ni and Zn may indicate the influence of diagenetic or hydrothermal processes [43]. Host lithologies that contain detrital components identified from their rounded appearance and association with characteristic detrital minerals may also contain detrital sulfide grains. Detrital sulfides are not expected to preserve information on the sulfur cycle in the depositional environment of the host rock. Occurrences of sulfide bands parallel to bedding or finely disseminated crystals in sedimentary rocks suggest that the sulfur is sedimentary in origin, whereas euhedral sulfide crystals may have grown during diagenesis and/or metamorphism from sedimentary sulfur. Finally, authigenic sulfides that incorporate sulfur from the environment of deposition can display ranges of $\delta^{34}S$ values, which are indicative of biological and/or non-biological oxido-reduction fractionation reactions at time of deposition. Because metamorphic recrystallization of sulfides can result in different crystal habits and/or increases in crystal size, it has been argued that sulfide morphology is generally a weak criterion to infer an authigenic origin [5].

All sulfur isotope analyses reported here were performed using the CAMECA ims 1270 multicollector ion microprobe at the University of California in Los Angeles following our usual procedures [5,7]. Ion

Table 3
Sulfur isotope data from standards

Grain spot*	^{32}S average intensity	$\delta^{34}S_{CDT}$ (‰)	$\pm 2\sigma^{\dagger}$ (‰)	$\delta^{33}S_{CDT}$ (‰)	$\pm 2\sigma^{\dagger}$ (‰)	$\Delta^{33}S$ (‰)	$\pm 2\sigma^{\dagger}$ (‰)
Session 1							
CDT (troilite)							
1b@1	3.62E+08	+0.86	1.09	+0.56	0.68	+0.12	0.28
1b@2	3.55E+08	−0.34	1.09	−0.08	0.69	+0.09	0.29
1c@1	4.11E+08	−0.14	1.09	+1.16	0.67	+0.22	0.26
1c@2	4.38E+08	−0.38	1.09	−0.21	0.67	−0.01	0.25
Trout Lake (chalcopyrite)							
2c@1	4.96E+08	+0.24	1.09	−0.08	0.66	−0.21	0.23
2c@2	5.10E+08	+0.30	1.09	−0.03	0.66	−0.18	0.23
2c@3	5.04E+08	+0.36	1.09	+0.19	0.66	0.00	0.22
Balmat (pyrite)							
4a@1	5.06E+08	+15.50	1.09	+7.98	0.66	−0.02	0.24
4a@2	4.99E+08	+15.47	1.09	+8.05	0.66	+0.07	0.23
4a@3	4.98E+08	+15.78	1.09	+8.16	0.66	+0.02	0.22
4c@1	5.86E+08	+15.14	1.09	+7.77	0.66	−0.04	0.24
4c@2	5.95E+08	+14.94	1.09	+7.83	0.66	+0.12	0.21
4c@3	6.27E+08	+15.01	1.09	+7.71	0.66	−0.04	0.23
4c@4	6.30E+08	+15.06	1.09	+7.85	0.65	+0.07	0.21
4c@5	5.31E+08	+14.66	1.09	+7.47	0.66	−0.10	0.24
4c@6	5.33E+08	+14.79	1.09	+7.60	0.66	−0.04	0.24
4c@7	5.53E+08	+14.91	1.09	+7.65	0.66	−0.05	0.21
4c@8	5.47E+08	+14.84	1.09	+7.60	0.66	−0.06	0.23
Anderson (pyrrhotite)							
5a@1	3.54E+08	+2.20	1.09	+1.13	0.68	−0.01	0.27
5a@2	3.68E+08	+2.04	1.09	+1.07	0.68	+0.01	0.28
5a@3	3.40E+08	+2.66	1.09	+1.14	0.69	−0.24	0.29
5a@4	4.17E+08	+1.41	1.09	+0.67	0.67	−0.06	0.26
5a@5	4.22E+08	+1.19	1.09	+0.62	0.67	0.00	0.26
5a@6	3.97E+08	+0.98	1.09	+0.45	0.66	−0.06	0.24
5a@7	3.90E+08	+1.22	1.09	+0.63	0.68	−0.01	0.28
5b@1	3.99E+08	+0.75	1.09	+0.58	0.67	+0.19	0.25
5b@2	3.96E+08	−0.26	1.09	−0.04	0.67	+0.09	0.25
5b@3	4.10E+08	+1.17	1.09	+0.60	0.67	−0.01	0.24
5b@4	4.06E+08	+1.45	1.09	+0.79	0.67	+0.04	0.25
5d@1	4.30E+08	+1.50	1.09	+0.74	0.67	−0.03	0.25
5d@2	4.48E+08	+1.34	1.09	+0.70	0.67	+0.01	0.25
AND@1	3.82E+08	+1.91	1.09	+1.11	0.67	+0.12	0.25
AND@2	4.24E+08	+1.43	1.09	+0.90	0.67	+0.15	0.26
Session 2							
CDT (troilite)							
1a@1	5.56E+08	−0.09	0.97	−0.11	0.55	−0.06	0.24
1a@2	5.56E+08	−0.66	0.98	−0.43	0.54	−0.09	0.22
1a@3	5.38E+08	+0.06	0.97	−0.02	0.54	−0.05	0.21
1a@4	5.55E+08	−0.10	0.97	−0.01	0.54	+0.04	0.23
1a@5	5.54E+08	−0.69	0.98	−0.30	0.54	+0.05	0.22
1a@6	5.69E+08	−0.44	0.97	−0.07	0.54	+0.16	0.22
1a@7	5.34E+08	+0.15	0.97	+0.03	0.54	−0.05	0.22
1a@8	4.12E+08	−0.83	0.98	−0.47	0.56	−0.04	0.25
1a@9	3.71E+08	−0.40	0.97	−0.27	0.57	−0.07	0.29
1a@10	3.77E+08	−1.31	0.98	−0.63	0.56	+0.05	0.26
1b@3	5.25E+08	+0.99	0.98	+0.45	0.55	−0.07	0.23
1b@4	5.09E+08	+0.48	0.98	+0.42	0.54	+0.17	0.21
1b@5	4.90E+08	+1.48	0.97	+0.85	0.55	+0.08	0.24
1b@6	4.22E+08	−0.25	0.97	−0.12	0.55	+0.01	0.23
1b@7	4.46E+08	−0.49	0.98	−0.17	0.55	+0.09	0.23
1b@8	4.73E+08	+0.19	0.98	0.00	0.55	−0.10	0.23

Table 3 (*continued*)

Grain spot*	^{32}S average intensity	$\delta^{34}S_{CDT}$ (‰)	$\pm 2\sigma^{\dagger}$ (‰)	$\delta^{33}S_{CDT}$ (‰)	$\pm 2\sigma^{\dagger}$ (‰)	$\Delta^{33}S$ (‰)	$\pm 2\sigma^{\dagger}$ (‰)
Session 2							
CDT (troilite)							
1b@9	4.89E+08	+0.04	0.98	0.00	0.55	−0.02	0.23
1b@10	4.97E+08	−0.31	0.98	−0.16	0.54	0.00	0.22
1b@11	4.08E+08	−1.22	0.98	−0.80	0.55	−0.17	0.25
CDT@1	3.69E+08	+1.54	0.98	+0.80	0.56	0.00	0.27
CDT@2	4.11E+08	+1.67	0.97	+0.76	0.58	−0.11	0.29
CDT@1	3.64E+08	+0.70	0.97	+0.32	0.56	−0.05	0.26
Trout Lake (chalcopyrite)							
2c@4	8.00E+08	+0.65	0.97	+0.28	0.53	−0.06	0.19
2c@5	7.43E+08	−0.93	0.97	−0.44	0.54	+0.04	0.21
2c@6	7.55E+08	+0.67	0.97	+0.44	0.54	+0.10	0.21
2c@7	7.60E+08	+0.60	0.97	+0.29	0.54	−0.02	0.22
2c@8	7.21E+08	−0.82	0.97	−0.41	0.54	+0.02	0.21
2c@9	6.43E+08	+0.58	0.97	+0.29	0.54	−0.01	0.21
2c@10	6.43E+08	+0.68	0.97	+0.44	0.55	+0.09	0.23
2c@11	6.01E+08	+0.35	0.98	+0.24	0.54	+0.06	0.21
TL_A@1	5.88E+08	+0.60	0.97	+0.23	0.54	−0.09	0.21
TL_A@2	5.95E+08	+0.58	0.98	+0.32	0.54	+0.02	0.22
TL_A@3	5.95E+08	+0.56	0.98	+0.27	0.55	−0.02	0.23
TL_A@4	6.00E+08	+0.53	0.98	+0.21	0.55	−0.06	0.23
TL_B@1	5.43E+08	+0.19	0.97	+0.13	0.54	+0.03	0.22
TL_B@2	5.62E+08	+0.28	0.98	+0.18	0.55	+0.03	0.23
TL_B@3	5.55E+08	+0.09	0.97	+0.20	0.54	+0.16	0.21
TL_B@4	5.57E+08	+0.19	0.98	+0.23	0.55	+0.14	0.23
Balmat (pyrite)							
4a@4	8.04E+08	+15.20	0.97	+7.78	0.54	−0.06	0.21
4a@5	7.97E+08	+15.05	0.97	+7.80	0.54	+0.03	0.21
4a@6	7.44E+08	+15.24	0.97	+8.01	0.54	+0.14	0.23
4a@7	7.66E+08	+15.01	0.97	+7.87	0.53	+0.13	0.20
4a@8	7.90E+08	+14.89	0.97	+7.68	0.53	0.00	0.20
4a@9	7.90E+08	+15.04	0.97	+7.81	0.53	+0.04	0.20
4a@10	8.00E+08	+15.15	0.97	+7.87	0.54	+0.05	0.21
4a@11	7.94E+08	+15.09	0.97	+7.78	0.54	−0.01	0.20
4a@12	8.01E+08	+15.19	0.97	+7.94	0.54	+0.10	0.20
4a@13	7.94E+08	+14.99	0.97	+7.77	0.54	+0.04	0.21
4a@14	6.60E+08	+15.10	0.97	+7.82	0.54	+0.03	0.22
4a@15	6.62E+08	+15.16	0.97	+7.88	0.54	+0.05	0.21
4a@16	6.70E+08	+15.20	0.97	+7.82	0.54	−0.02	0.22
4b@1	7.59E+08	+14.60	0.97	+7.66	0.54	+0.13	0.21
4b@2	7.75E+08	+15.12	0.97	+7.82	0.54	+0.01	0.21
4b@3	7.98E+08	+15.17	0.97	+7.82	0.54	−0.01	0.21
4b@4	8.17E+08	+15.21	0.97	+7.80	0.53	−0.05	0.20
4b@5	8.14E+08	+15.20	0.97	+7.79	0.53	−0.06	0.20
4b@6	6.79E+08	+15.28	0.97	+7.93	0.54	+0.04	0.22
4b@7	6.83E+08	+15.27	0.97	+7.94	0.54	+0.06	0.20
4b@8	7.26E+08	+15.22	0.97	+7.76	0.53	−0.09	0.20
4c@9	7.45E+08	+15.07	0.97	+7.67	0.54	−0.11	0.21
4c@10	6.21E+08	+15.28	0.97	+7.89	0.54	0.00	0.21
4c@11	6.25E+08	+15.19	0.97	+7.94	0.54	+0.10	0.21
4c@12	6.00E+08	+15.02	0.98	+7.85	0.54	+0.09	0.22
4c@13	6.15E+08	+14.96	0.97	+7.79	0.54	+0.07	0.21
4c@14	6.13E+08	+14.96	0.98	+7.68	0.54	−0.04	0.22
4c@15	6.19E+08	+14.92	0.98	+7.62	0.55	−0.08	0.23
4c@16	5.63E+08	+15.05	0.98	+7.54	0.55	−0.23	0.24
4c@17	5.54E+08	+15.02	0.98	+7.79	0.54	+0.04	0.22
4c@18	5.52E+08	+14.67	0.97	+7.81	0.54	+0.24	0.21

(continued on next page)

Table 3 (*continued*)

Grain spot*	^{32}S average intensity	$\delta^{34}S_{CDT}$ (‰)	$\pm 2\sigma^{\dagger}$ (‰)	$\delta^{33}S_{CDT}$ (‰)	$\pm 2\sigma^{\dagger}$ (‰)	$\Delta^{33}S$ (‰)	$\pm 2\sigma^{\dagger}$ (‰)
Session 2							
Balmat (pyrite)							
4d@2	7.99E+08	+14.61	0.97	+7.65	0.54	+0.10	0.21
4d@3	7.87E+08	+14.59	0.97	+7.65	0.54	+0.12	0.21
4d@4	5.97E+08	+15.23	0.98	+7.81	0.54	−0.05	0.22
4d@5	5.85E+08	+15.22	0.97	+7.91	0.54	+0.05	0.22
4d@6	5.92E+08	+15.09	0.97	+7.91	0.55	+0.12	0.23
4d@7	5.92E+08	+15.13	0.97	+7.96	0.55	+0.15	0.23
4d@8	5.86E+08	+14.97	0.97	+7.71	0.55	−0.02	0.23
4d@9	6.04E+08	+15.00	0.97	+7.67	0.54	−0.08	0.22
4d@10	5.78E+08	+15.14	0.98	+7.76	0.55	−0.05	0.23
4d@11	6.09E+08	+15.05	0.98	+7.78	0.54	+0.02	0.22
4d@12	5.66E+08	+15.36	0.97	+7.76	0.55	−0.17	0.24
4d@13	5.60E+08	+15.30	0.97	+7.84	0.54	−0.06	0.22
4d@14	5.63E+08	+15.33	0.97	+8.14	0.55	+0.23	0.23
4d@15	5.51E+08	+15.39	0.98	+7.98	0.54	+0.04	0.23
4d@16	5.34E+08	+15.19	0.97	+7.79	0.54	−0.05	0.22
4d@17	5.85E+08	+15.29	0.97	+7.85	0.54	−0.04	0.23
4d@18	5.43E+08	+15.24	0.97	+7.78	0.55	−0.08	0.24
4d@19	5.67E+08	+15.15	0.97	+7.85	0.54	+0.03	0.23
4d@20	5.02E+08	+15.26	0.98	+8.13	0.54	+0.26	0.22
4d@21	5.43E+08	+15.06	0.97	+7.80	0.54	+0.03	0.23
Anderson (pyrrhotite)							
5a@1	5.57E+08	+1.54	0.97	+0.64	0.55	−0.15	0.24
5a@2	5.39E+08	+1.16	0.98	+0.60	0.55	0.00	0.23
5a@8	5.68E+08	+1.96	0.97	+1.07	0.54	+0.05	0.21
5a@9	5.77E+08	+2.03	0.97	+1.03	0.54	−0.01	0.22
5a@10	5.38E+08	+1.56	0.98	+0.82	0.54	+0.02	0.21
5a@11	5.60E+08	+1.81	0.97	+0.87	0.55	−0.07	0.24
5a@12	5.70E+08	+1.41	0.97	+0.71	0.54	−0.02	0.21
5a@13	5.65E+08	+1.64	0.97	+0.80	0.55	−0.05	0.23
5a@14	5.92E+08	+1.75	0.97	+0.97	0.54	+0.07	0.22
5a@15	5.57E+08	+1.61	0.97	+0.96	0.55	+0.13	0.23
5a@16	5.47E+08	+1.31	0.97	+0.79	0.54	+0.11	0.20
5b@5	5.62E+08	+1.30	0.98	+0.73	0.54	+0.06	0.22
5b@6	5.37E+08	+2.05	0.97	+0.98	0.54	−0.08	0.22
5b@7	5.33E+08	+1.82	0.98	+0.90	0.55	−0.04	0.24
5b@8	5.42E+08	+1.64	0.97	+0.73	0.55	−0.12	0.23
5b@9	6.03E+08	+0.49	0.97	+0.24	0.54	−0.01	0.22
5b@10	6.31E+08	+1.24	0.97	+0.64	0.54	0.00	0.22
5b@11	5.26E+08	+1.43	0.98	+0.67	0.54	−0.07	0.23
5b@12	5.40E+08	+1.87	0.97	+1.05	0.54	+0.08	0.22
5b@13	5.62E+08	+1.85	0.97	+0.95	0.54	−0.01	0.23
5b@14	5.47E+08	+1.52	0.97	+0.78	0.55	−0.01	0.23
5b@15	4.32E+08	+0.45	0.98	+0.27	0.55	+0.04	0.24
5b@16	4.24E+08	+0.97	0.98	+0.37	0.56	−0.13	0.26
5b@17	4.49E+08	+1.32	0.98	+0.63	0.55	−0.05	0.24
5b@18	4.40E+08	+1.03	0.97	+0.31	0.54	−0.23	0.21
5b@19	4.39E+08	+1.03	0.97	+0.50	0.56	−0.03	0.26
5c@1	4.44E+08	+1.37	0.98	+0.81	0.55	+0.10	0.23
5c@2	4.28E+08	−0.31	0.98	−0.08	0.57	+0.08	0.28
5c@3	4.16E+08	+0.66	0.97	+0.18	0.56	−0.16	0.26
5d@3	4.13E+08	+1.45	0.98	+0.78	0.56	+0.03	0.26
5d@4	4.39E+08	+1.61	0.98	+0.75	0.55	−0.08	0.23
5d@5	4.46E+08	+1.39	0.98	+0.60	0.55	−0.12	0.24
5e@1	4.11E+08	+1.48	0.97	+0.80	0.57	+0.04	0.28
5e@2	4.13E+08	+1.13	0.98	+0.42	0.56	−0.16	0.26
5e@3	4.13E+08	+1.92	0.98	+1.02	0.56	+0.02	0.26

microprobe analyses of unknown sulfides were bracketed by measurements of standards of compositionally equivalent sulfide phases. Instrumental methods involved the use of a liquid nitrogen cold trap in the sample chamber as previously described [5,7] except as follows. The average time per analysis was approximately 500 s, and consisted of 200 s of pre-sputtering, 30 cycles of data acquisition each of 5 s and about 150 s of setup time between analyses. Each of the two analytical sessions was independently processed because different instrument conditions lead to different instrumental mass fractionation. Data reduction can be summarized as follows (see [5] for details of this procedure): (1) subtraction of the averaged detector baseline from the secondary-ion beam intensities; (2) calculation of the $^{34}S/^{32}S$ instrumental mass-fractionation ($IMF_{34/32}$) for each standard by taking the ratio of the mean, baseline-corrected instrumental $^{34}S/^{32}S$ value to the independently measured value; and (3) correction of all analyses for IMF by dividing the baseline-corrected ratio by the IMF for the corresponding phase. The instrumental mass-fractionation for the $^{33}S/^{32}S$ ratio ($IMF_{33/32}$) was calculated from $IMF_{34/32}$ by assuming an exponential law [44], so that $IMF_{33/32}=(IMF_{34/32})^{\ln(m33/m32)/\ln(m34/m32)}$, where m32, m33, and m34 are the masses of ^{32}S, ^{33}S, and ^{34}S respectively. Detector baselines measured periodically throughout the sessions showed no significant drift with time, so averaged values were used for baseline correction. Internal standard errors for each analysis were calculated from 30 pairs of ratios, one pair per measurement cycle. The overall reported error on delta-values is the combination of the internal and external error, which in all analyses is dominated by the latter.

4. Results

Electron microprobe analyses were performed on selected sulfides (Table 2) and phases present included pyrite, pyrrhotite and chalcopyrite. Two pyrite grains from sample *SM0017_1634.9* had about 2 wt.% Ni and similar Ni-enrichments were also observed in samples *SM0017_1539.6* (up to 5.4 wt.% in one grain), *SM0175_1388.5* and *SM0175_1383.5*. Pyrite in the Nipissing Diabase had between 0.4 and 1.5 wt.% Co and a few pyrite grains from two samples of the Espanola Fm. (*SM0175_839.6* and *SM0017_848.0*) had between 2 and 3% Co. Levels of Zn were measured to be less than 0.1 wt.% in all analyzed sulfides. Characterization of sulfide targets by optical and electron microscopy is shown in Fig. 2. This step preceded isotopic analyses by ion microprobe and the results for analyses of standards and Huronian sulfides are shown in Tables 3 and 4, respectively. In contrast to published sulfur isotope data for Huronian sediments [2,11,39,40] (Table 5), our new high-spatial resolution measurements permit direct petrographic control of the analyzed sulfides and preserve information on crystal morphologies. A York regression [45] through all the standard measurements was calculated to determine the experimental slope λ and the $(^{33}S/^{32}S)_{CDT}$:

	n (# std)	$\lambda \pm 2\sigma$	MSWD	$(^{33}S/^{32}S)_{CDT}$
Session 1	33	0.5184±0.0049	1.6	0.007883
Session 2	124	0.5196±0.0022	1.8	0.007883

The calculated slopes agree within error with the value of $\lambda=0.518$ commonly obtained from ion microprobe analyses on "natural standards". Because this slope is consistent with hundreds of published analyses on standard sulfides collected so far by ion microprobe, we adopt a slope of 0.518 for the calculation of $\Delta^{33}S$ values. We acknowledge however that this value differs slightly from the more commonly used $\lambda=0.515$. The latter is an approximation that stems from calculations of fractionation factors for equilibrium reactions and sulfur isotope exchange reactions, which typically yield slopes closer to 0.515 [46,47]. Compared to the value of 0.515 for the MDF slope, the choice of a 0.518 slope has an insignificant effect on our calculated $\Delta^{33}S$ values (a difference of 0.012±0.019‰ (1σ) on average) or in the interpretation of the data, but we acknowledge that this difference is non-negligible for high precision analyses by the SF_6 method (e.g. [48]). The current uncertainty in the determination of λ and the minor difference between inter-laboratory analyses may eventually be resolved through the development of new sulfide standards. The MSWD is based on the internal errors and the 2σ error on the slope was augmented by the square-root of the MSWD. The York regression was also used to generate a MDF band in ($\delta^{34}S_{CDT}$, $\delta^{33}S_{CDT}$)-space [5], which is defined by curves with a 2σ width of ~±0.2‰ about the slope of 0.518 (Fig. 3). Delta-values that plot outside of the MDF band in a three-isotope plot are considered to carry resolvable MIF sulfur isotope signatures.

Notes to Table 3:

*Grain spot name begins with a number for the standard (1=CDT; 2=Trout Lake; 4=Balmat; 5=Anderson) and a letter for specific grains, followed by @number, which designates the spot number on that grain.†The 2σ errors for the delta-values are calculated by taking the quadratic of the internal and external errors. The external error is the reproducibility of the standards and dominates over the internal error.

4.1. Results for Huronian sedimentary rocks

A thin argillaceous bed immediately below the contact with the Matinenda Fm., and above altered metavolcanic rocks, contained layered pyrite blebs and finely disseminated anhedral pyrrhotite grains (Fig. 2). These sulfides are not unambiguously authigenic and have near-zero $\Delta^{33}S$ and $\delta^{34}S$ values indistinguishable from magmatic sources of sulfur (Fig. 4). As described above, immediately before the first Huronian glaciation, pelitic sediments of the McKim Fm. were deposited in a deep-lacustrine or marine setting. Samples of argillites in the McKim Fm. either contain rounded detrital sulfide grains associated with other detrital minerals or authigenic anhedral crystals in a fine-grained micaceous matrix and sulfide bands that occur parallel to bedding. Detrital sulfide grains occur in a clastic bed of the argillaceous quartzite *SM0017_1590.8* and have $\Delta^{33}S$ values between +0.26 and +0.47‰ (Fig. 4). Because these are detrital grains, they could have originated from an Archean sedimentary rock and therefore would have no environmental implications for the time of McKim sedimentation. Finely disseminated anhedral pyrite and pyrrhotite grains in McKim argillite samples *SM0017_1539.6* and *SM0175_1542.0* were interpreted to be authigenic. These were found to have a small range of low $\delta^{34}S$ values and a range of $\Delta^{33}S$ values between −0.31 and +0.39‰ (Table 4; Fig. 2). Such a 0.7‰ range in $\Delta^{33}S$ in these McKim argillite samples suggests small MIF deviations at time of sedimentation. The highly deformed amphibolite grade metapelite *HU0415* from the McKim Fm. collected immediately south of the Murray Fault (Fig. 1), contains subhedral pyrrhotite and chalcopyrite crystals that have $\Delta^{33}S$ values between +0.55 and +0.78‰ (Fig. 2). Because of the high level of deformation and alteration of this rock, the origin of these sulfides remains equivocal as they could be authigenic or detrital. Therefore we regard the MIF signatures recorded in these sulfides as not necessarily representative of environmental conditions during deposition.

The glacial diamictite of the Ramsey Lake Fm. is correlative with the Paleoproterozoic diamictite of the Vagner Fm. in the Snowy Pass Supergroup, Wyoming [14,17,49]. Argillites of the Pecors Fm. occur stratigraphically above this first diamictite and contain sulfide bands and anhedral crystals distributed parallel to finely laminated beds. The Pecors sulfides are interpreted to be authigenic on the basis of their host lithologies, mode of occurrence and from the lack of evidence for a detrital input based on co-existing phases. For example, pyrrhotite blebs in Pecors sample *SM0175_1420.1* and anhedral pyrite grains in *SM0175_1388.5* are interpreted to be authigenic because they occur parallel to schistosity in an argillite that does not contain characteristic large detrital grains (e.g. rounded zircons, quartz, etc.). Pyrrhotite bands in argillite samples *SM0175_1413.8*, *SM0175_1383.5* and *SM0175_1368.1* are also interpreted to be authigenic because they occur as finely laminated beds parallel to bedding. Lastly, finely disseminated microcrystalline pyrrhotite in Pecors sample *SM0175_1375.4* occurs as centimeter-sized rounded aggregates, which we interpret to be the result of post-depositional processes. In all six Pecors Fm. samples collected over ~50 m of core section, twenty-four analyses on 18 individual sulfides were performed. These analyses show a range of $\Delta^{33}S$ values between −0.07 and +0.88‰ (Fig. 2), out of which only three analyses of pyrrhotite bands or grains showed MIF $\Delta^{33}S$ values between +0.45 and +0.88‰. However, these three sulfides are significant because they are interpreted to be authigenic in origin.

The second Huronian glaciation is represented by the Bruce diamictite and is correlated with the Vagner diamictite in the Snowy Pass Supergroup (Wyoming) [49]. Overlying the Bruce diamictite is the Espanola cap carbonate with characteristic negative $\delta^{13}C_{carb}$ values [17]. The core *KERR-McGEE 156-1* (SM0175) exhibits four mafic Nipissing intrusions within the Espanola carbonate including divisions between the Bruce and Gowganda diamictites. A total of thirteen analyses on ten pyrite grains were performed on sulfides from the first carbonate layer (interbedded between Nipissing intrusions) and four analyses were performed on euhedral pyrites from an Espanola siltstone in core *KERR-McGEE 150-4* (SM0017). Euhedral to subhedral pyrite crystals in Espanola carbonates and siltstones were found to have a large range of $\delta^{34}S$ values between +1.7 and +31.2‰ (Fig. 2). These results differ significantly from the near-zero $\delta^{34}S$ values for the Nipissing diabase (Fig. 4b), which suggests that the mafic intrusions did not influence the sulfur isotope composition of sulfides in the carbonate. The highly variable $\delta^{34}S$ values in pyrite from carbonates suggest MDF processes operational at the time of sedimentation and therefore represent a sedimentary source of sulfur. Silicate inclusions occur in some subhedral pyrite grains from sample *SM0175_839.6* and were likely incorporated during metamorphic recrystallization of sulfides. In addition to the positive $\delta^{34}S$ values up to +31‰, Espanola sulfides have $\Delta^{33}S$ values that vary between −0.20 and +0.13‰ (Table 5). This is significant because it suggests that the demise of small (remnant or transient?) MIF signatures in Pecors sediments occurred between the Ramsey Lake and Bruce glaciations.

Table 4
Sulfur isotope data for Huronian sulfides

Grain spot*	Phase	Interpreted origin	^{32}S average intensity	$\delta^{34}S_{CDT}$ (‰)	$\pm 2\sigma^{\dagger}$ (‰)	$\delta^{33}S_{CDT}$ (‰)	$\pm 2\sigma^{\dagger}$ (‰)	$\Delta^{33}S$ (‰)	$\pm 2\sigma^{\dagger}$ (‰)
Session 1									
SM0017_1634.9a@1	Po	Ambiguous	3.43E+08	+0.82	1.09	+0.53	0.68	+0.11	0.28
SM0017_1634.9b@1	Po	Ambiguous	3.87E+08	−0.55	1.09	−0.13	0.67	+0.15	0.26
SM0017_1634.9c@1	Py	Ambiguous	5.81E+08	−1.25	1.09	−0.44	0.66	+0.21	0.23
SM0017_1634.9d@1	Py	Ambiguous	6.04E+08	−0.77	1.09	−0.17	0.66	+0.22	0.22
SM0017_1634.9d@2	Py	Ambiguous	5.86E+08	−1.57	1.09	−0.60	0.66	+0.21	0.22
SM0017_1590.8a@1	Po	Detrital	3.65E+08	+1.71	1.09	+1.21	0.67	+0.33	0.25
SM0017_1590.8a@2	Po	Detrital	3.77E+08	+1.44	1.09	+1.06	0.70	+0.31	0.32
SM0017_1590.8b@1	Po	Detrital	3.70E+08	+1.52	1.09	+1.05	0.67	+0.26	0.25
SM0017_1590.8d@1	Po	Detrital	3.59E+08	+1.35	1.09	+1.16	0.68	+0.47	0.28
SM0175_855.9a@1	Py	Authigenic	5.68E+08	+25.12	1.09	+12.82	0.66	−0.12	0.23
SM0175_855.9b@1	Py	Authigenic	4.02E+08	+28.29	1.09	+14.35	0.68	−0.20	0.27
SM0175_855.9d@1	Py	Authigenic	2.89E+08	+26.48	1.09	+13.44	0.69	−0.19	0.30
Session 2									
SM0017_1539.6a@1	Py	Authigenic	6.72E+08	+1.43	0.98	+0.99	0.54	+0.25	0.21
SM0017_1539.6b@1	Py	Authigenic	5.35E+08	+0.13	0.98	+0.41	0.55	+0.34	0.25
SM0017_1539.6c@1	Py	Authigenic	7.67E+08	+1.79	0.97	+1.23	0.53	+0.31	0.20
SM0017_1539.6d@1	Py	Authigenic	6.95E+08	+1.03	0.98	+0.92	0.54	+0.39	0.22
SM0017_848.0a@1	Py	Authigenic	5.68E+08	+2.17	0.97	+1.17	0.53	+0.05	0.20
SM0017_848.0b@1	Py	Authigenic	6.18E+08	+2.97	0.98	+1.50	0.54	−0.04	0.23
SM0017_848.0c@1	Py	Authigenic	6.20E+08	+2.65	0.97	+1.46	0.53	+0.09	0.20
SM0017_848.0d@1	Py	Authigenic	6.31E+08	+1.69	0.97	+0.84	0.54	−0.03	0.22
SM0175_1542.0c@1	Po	Authigenic	3.66E+08	+0.94	0.98	+0.82	0.56	+0.33	0.27
SM0175_1542.0c@2	Po	Authigenic	1.17E+08	+0.43	0.99	+0.24	0.72	+0.01	0.52
SM0175_1542.0c@3	Po	Authigenic	1.37E+08	−0.63	0.98	−0.63	0.65	−0.31	0.43
SM0175_1542.0d@1	Po	Authigenic	1.78E+08	+1.08	0.98	+0.73	0.58	+0.17	0.29
SM0175_1542.0d@2	Po	Authigenic	3.91E+08	+1.59	0.98	+1.00	0.56	+0.18	0.26
SM0175_1542.0d@3	Po	Authigenic	1.70E+08	+1.01	0.98	+0.83	0.67	+0.31	0.45
SM0175_1420.1a@1	Po	Authigenic	5.92E+08	+4.93	0.97	+2.66	0.54	+0.11	0.22
SM0175_1420.1b@1	Po	Authigenic	5.82E+08	+5.60	0.97	+3.08	0.55	+0.18	0.23
SM0175_1420.1c@1	Po	Authigenic	5.91E+08	+5.57	0.97	+3.10	0.54	+0.22	0.22
SM0175_1420.1c@2	Po	Authigenic	5.90E+08	+5.57	0.97	+3.03	0.54	+0.14	0.22
SM0175_1413.8a@1	Po	Authigenic	5.31E+08	+5.57	0.97	+3.09	0.55	+0.21	0.24
SM0175_1413.8a@2	Po	Authigenic	5.45E+08	+5.64	0.97	+3.09	0.55	+0.18	0.24
SM0175_1413.8d@1	Po	Authigenic	5.52E+08	+5.85	0.98	+3.28	0.55	+0.26	0.23
SM0175_1413.8e@1	Po	Authigenic	5.54E+08	+5.61	0.97	+2.98	0.54	+0.08	0.21
SM0175_1388.5a@1	Py	Authigenic	7.27E+08	+3.86	0.97	+2.16	0.54	+0.16	0.22
SM0175_1388.5b@1	Py	Authigenic	7.49E+08	+3.70	0.97	+2.00	0.53	+0.09	0.20
SM0175_1388.5c@1	Py	Authigenic	6.87E+08	+3.61	0.97	+2.06	0.54	+0.19	0.20
SM0175_1388.5c@2	Py	Authigenic	7.35E+08	+3.15	0.98	+1.79	0.54	+0.16	0.21
SM0175_1383.5a@1	Po	Authigenic	4.12E+08	+4.94	0.98	+2.84	0.56	+0.28	0.25
SM0175_1383.5a@2	Po	Authigenic	4.42E+08	+5.18	0.98	+2.61	0.56	−0.07	0.26
SM0175_1383.5b@1	Py	Authigenic	5.93E+08	+3.41	0.97	+2.03	0.54	+0.27	0.20
SM0175_1383.5c@1	Po	Authigenic	4.09E+08	+3.68	1.00	+2.79	0.55	+0.88	0.23
SM0175_1375.4d@1	Po	Authigenic	1.25E+08	+4.43	0.98	+2.64	0.80	+0.34	0.63
SM0175_1375.4d@2	Po	Authigenic	2.69E+08	+5.80	0.98	+3.04	0.60	+0.04	0.35
SM0175_1375.4e@1	Po	Authigenic	1.25E+08	+4.55	0.98	+2.70	0.76	+0.35	0.58
SM0175_1375.4f@1	Ch	Authigenic	1.70E+08	−0.28	0.98	−0.21	0.68	−0.07	0.46
SM0175_1368.1a@1	Po	Authigenic	4.04E+08	+6.41	0.97	+3.46	0.56	+0.15	0.25
SM0175_1368.1b@1	Po	Authigenic	4.29E+08	+5.63	0.98	+2.96	0.54	+0.05	0.22
SM0175_1368.1b@2	Po	Authigenic	4.46E+08	+5.81	0.97	+3.46	0.55	+0.45	0.25
SM0175_1368.1c@1	Po	Authigenic	4.30E+08	+6.53	0.97	+3.88	0.55	+0.51	0.23
SM0175_861.4a@1	Py	Authigenic	7.89E+08	+29.09	0.97	+14.98	0.54	+0.02	0.20
SM0175_861.4a@2	Py	Authigenic	7.77E+08	+31.19	0.97	+16.16	0.54	+0.13	0.22
SM0175_861.4b@1	Py	Authigenic	7.54E+08	+31.15	0.97	+16.08	0.54	+0.07	0.21
SM0175_861.4b@2	Py	Authigenic	7.63E+08	+29.27	0.97	+15.11	0.54	+0.05	0.21

(continued on next page)

Table 4 (*continued*)

Grain spot*	Phase	Interpreted origin	^{32}S average intensity	$\delta^{34}S_{CDT}$ (‰)	$\pm 2\sigma^{\dagger}$ (‰)	$\delta^{33}S_{CDT}$ (‰)	$\pm 2\sigma^{\dagger}$ (‰)	$\Delta^{33}S$ (‰)	$\pm 2\sigma^{\dagger}$ (‰)
Session 2									
SM0175_851.2@1	Py	Authigenic	4.89E+08	+3.65	0.98	+1.74	0.55	−0.14	0.24
SM0175_851.2@2	Py	Authigenic	5.02E+08	+3.65	0.98	+1.94	0.55	+0.05	0.23
SM0175_839.6a@1	Py	Authigenic	5.86E+08	+11.95	0.97	+6.12	0.54	−0.05	0.23
SM0175_839.6d@1	Py	Authigenic	4.83E+08	+11.37	0.97	+5.87	0.54	−0.01	0.22
SM0175_839.6e@1	Py	Authigenic	3.13E+08	+12.75	0.98	+6.58	0.57	0.00	0.29
SM0175_839.6f@1	Py	Authigenic	5.40E+08	+13.11	0.97	+6.75	0.54	−0.02	0.20
SM0175_819.2a@1	Py	Magmatic	5.31E+08	+0.04	0.98	+0.02	0.55	0.00	0.23
SM0175_819.2a@2	Py	Magmatic	5.58E+08	−0.06	0.97	+0.02	0.55	+0.05	0.24
SM0175_819.2b@1	Py	Magmatic	3.36E+08	+0.44	0.98	+0.15	0.58	−0.08	0.31
SM0175_819.2c@1	Py	Magmatic	5.91E+08	+0.19	0.97	+0.12	0.54	+0.03	0.22
SM0060_261.2a@1	Py	Ambiguous	7.02E+08	+1.77	0.98	+1.03	0.54	+0.11	0.22
SM0060_261.2b@1	Py	Ambiguous	6.70E+08	+1.04	0.97	+0.71	0.55	+0.17	0.24
SM0060_261.2b@2	Py	Ambiguous	7.34E+08	+1.41	0.97	+0.81	0.54	+0.08	0.21
SM0060_261.2c@1	Py	Ambiguous	7.56E+08	−5.18	0.97	−2.51	0.54	+0.17	0.21
SM0060_261.2d@1	Py	Ambiguous	7.78E+08	+0.35	0.97	+0.27	0.54	+0.09	0.21
SM0406_635.8a@1	Py	Authigenic	8.34E+08	−12.51	0.97	−6.30	0.53	+0.21	0.19
SM0406_635.8b@1	Py	Authigenic	7.99E+08	−8.37	0.97	−4.17	0.54	+0.17	0.20
SM0406_635.8c@1	Py	Authigenic	8.00E+08	−7.06	0.97	−3.47	0.53	+0.19	0.20
SM0406_635.8d@1	Py	Authigenic	7.10E+08	−8.77	0.97	−4.35	0.54	+0.20	0.22
SM0406_635.8e@1	Py	Authigenic	7.52E+08	−8.57	0.97	−4.31	0.54	+0.14	0.21
HU0415a@1	Po	Ambiguous	5.30E+08	+0.71	0.97	+0.92	0.55	+0.55	0.23
HU0415b@1	Po	Ambiguous	5.42E+08	+1.51	0.97	+1.42	0.55	+0.63	0.23
HU0415c@1	Po	Ambiguous	5.03E+08	+0.85	0.98	+1.05	0.54	+0.61	0.22
HU0415d@1	Ch	Ambiguous	7.45E+08	+2.00	0.97	+1.76	0.54	+0.72	0.21
HU0415e@1	Ch	Ambiguous	6.47E+08	+1.90	0.97	+1.76	0.55	+0.78	0.23
HU0407a@1	Py	Authigenic	5.68E+08	+22.77	0.97	+11.74	0.54	0.00	0.22
HU0407b@1	Py	Authigenic	5.22E+08	+23.48	0.98	+11.99	0.56	−0.11	0.25
HU0407c@1	Py	Authigenic	5.51E+08	+11.34	0.97	+5.87	0.55	+0.01	0.24
HU0407d@1	Py	Authigenic	5.13E+08	+25.91	0.97	+13.19	0.56	−0.15	0.27

*Grain spot names begin with the sample number and a letter for specific grains, followed by @number, which designates the spot number on that grain.

†The 2σ errors for the delta-values are calculated by taking the quadratic of the internal and external errors. The external error is the reproducibility of the standards and dominates over the internal error.

The overlying Cobalt Group begins with the Gowganda Fm., the thickest of all three Huronian diamictites. Several Paleoproterozoic glacial diamictites in North America may be correlative with the Gowganda Fm. and are found in the Snowy Pass, Marquette (Michigan), Mistassini (Québec) and Hurwitz (Nunavut) supergroups [49]. Stratigraphically above the Gowganda diamictite is the Lorrain Fm., which was sampled in the core *Canadian Johns Manville 157-68-1* (SM0406). Five euhedral pyrite crystals were analyzed from a sample of Lorrain argillaceous bed associated with detrital quartz. Analyses revealed $\delta^{34}S$ values between −12.5 and −7.1‰ and $\Delta^{33}S$ between +0.14 and +0.21‰ consistent with previous results [40] (Table 5; Fig. 4). These $\delta^{34}S$ values indicate that MDF processes produced sulfide at the time of deposition and therefore are diagnostic of authigenic pyrite. Cherts from the overlying Gordon Lake Fm. are known to have primary anhydrite nodules with $\delta^{34}S_{sulfate}$ values between +12.3 and +15.6‰ and radiogenic $^{87}Sr/^{86}Sr$ ratios indicative of significant input from continental erosion [39]. Sample *SM0060_261.2* is an argillaceous quartzite from the Gordon Lake Fm. and contains rounded pyrite grains with silicate inclusions and near-zero $\Delta^{33}S$ values and $\delta^{34}S$ values between −5.2 and +1.8‰. Because these sulfides may be detrital or authigenic, their isotopic compositions may not relate to environmental conditions during sedimentation. Pyrite blebs more than 0.5 mm in size from red and banded cherty argillites in Gordon Lake sample *HU0407* are closely associated with large monazite crystals (circled in the image for *HU0407b* of Fig. 2) and oolites with rims of microcrystalline euhedral pyrite. These are essentially identical to the oolitic chamosites with fine grained pyrite described by Chandler [32]. These pyrites are deemed to be authigenic because they occur parallel to bedding and have $\delta^{34}S$ values between +11.3 and +25.9‰ (Fig. 2).

Table 5
Ranges of new and published $\Delta^{33}S$ and $\delta^{34}S$ values for Huronian sulfides and sulfate

Formation	New $\Delta^{33}S_{sulfide}$ [¶]	New $\delta^{34}S_{sulfide}$ [¶]	Published $\Delta^{33}S$ values [*,†]	Published $\delta^{34}S$ values [§,†]
Cobalt Group				
Gordon Lake	−0.15 to +0.17	−5.2 to +25.9	N.D.[#]	−10.6 to +7.6 (1)
Lorrain	+0.14 to +0.21	−12.5 to −7.1	N.D.[#]	−20.4 to +18.2 (1)
Gowganda	N.D.[#]	N.D.[#]	+0.15 (2)	−1.9 to +5.0 (1)
Quirke Lake Group				
Serpent	N.D.[#]	N.D.[#]	N.D.[#]	−0.1 to +1.2 (1)
Espanola	−0.20 to +0.13	+1.7 to +31.2	+0.34‰ (2)	+0.3 to +9.9 (1, 3)
Bruce	N.D.[#]	N.D.[#]	N.D.[#]	N.D.[#]
Hough Lake Group				
Mississagi	N.D.[#]	N.D.[#]	N.D.[#]	+0.2 to +2.4 (1)
Pecors	−0.07 to +0.88	−0.3 to +6.5	+0.07 (2)	−0.9 to +1.9 (1)
Ramsey Lake	N.D.[#]	N.D.[#]	N.D.[#]	−1.0 to +3.6 (1)
Elliot Lake Group				
McKim	−0.31 to +0.78	−0.6 to +2.0	N.D.[#]	−0.3 to +4.0 (1)
Matinenda	+0.11 to +0.22	−1.6 to +0.8	+0.04 (2)	−1.5 to +1.2 (1)
Livingstone Creek	N.D.[#]	N.D.[#]	N.D.[#]	N.D.[#]

Note: All ranges of delta-values are expressed in ‰.
[¶]Ranges shown are for all new data.
*Currently published $\Delta^{33}S$ values of Huronian rocks are for sulfate only.
[§]Only published $\delta^{34}S_{sulfide}$ values are shown (see text for relevant $\delta^{34}S_{sulfate}$ values).
[†](1) — Hattori et al. [40], (2) — Farquhar et al. [2], (3) — Bottomley et al. [11].
[#]N.D.=no data.

These analyses also revealed near-zero $\Delta^{33}S$ values between −0.15 and +0.17‰.

5. Discussion

5.1. Authigenecity of sulfides in Huronian sedimentary rocks

Based on our analysis, we view the demise of large magnitude MIF sulfur isotopes in the Paleoproterozoic geological record as a consequence of the accumulation of O_2 in the atmosphere at that time. Because isotopic dilution during sedimentation or post-depositional processes can result in a decrease of the intensity of $\Delta^{33}S$ deviations, an assessment of sulfide authigenecity in sedimentary rocks is of critical importance to the interpretation of multiple sulfur isotopes in the early Paleoproterozoic. Authigenetic-sedimentary sulfides are considered to contain sedimentary sulfur and their shapes and sizes vary according to diagenetic and metamorphic processes. As described before, the authigenecity of Huronian sulfides was interpreted on the basis of trace metal chemistry, isotopic composition, host lithology and mode of occurrence. A few sulfides in lower Huronian samples *SM0017_1634.9*, *SM0017_1539.6*, *SM0175_1388.5* and *SM0175_1383.5* contain between 1 and 2% Ni, while a few pyrite grains from Espanola samples *SM0175_839.6* and *SM0017_848.0* had between 2 and 3% Co. Such Ni and Co contents may have been incorporated during diagenesis or metamorphism. Detrital sulfides may carry information on atmospheric sulfur cycling if their source rocks were originally sedimentary and Archean in age, but this is irrelevant for the Paleoproterozoic sulfur cycle during sedimentation. For instance, detrital pyrrhotite grains in sample *SM0017_1590.8* were rounded and co-occurred with other characteristic detrital minerals such as large rounded quartz grains. Detrital sulfides in *SM0017_1590.8* were found to have $\Delta^{33}S$ values between +0.26 and +0.47‰, which represent small deviations from MDF, possibly from an Archean sedimentary rock. With the exception of spherical sulfide concretions, the shape of sulfide crystals does not appear to be a reliable diagnostic of sulfide authigenecity in Paleoproterozoic sedimentary rocks (see also [5]). Multicollector ion microprobe analyses of sulfides allow petrographic analysis of host lithologies and mode of occurrence of sulfides in sedimentary rocks. Furthermore, ion microprobe analyses can reveal ranges of sulfur isotope compositions that may occur between different grains in individual rock samples. While this analytical method is well suited for sulfides in Huronian sedimentary rocks, we also believe that multiple sulfur isotope analyses by laser fluorination methods could provide complementary information to evaluate authigenecity. This is because the higher precision and sensitivity for the measurement of both ^{33}S and ^{36}S with multicollector IRM GCMS can provide additional clues on biological processes and environmental conditions [50]. These high precision measurements have also revealed small $\Delta^{33}S$ deviations resolved for carbonate-associated sulfate in Proterozoic sedimentary rocks, which were interpreted to indicate microbial sulfur disproportionation at the time of deposition [51].

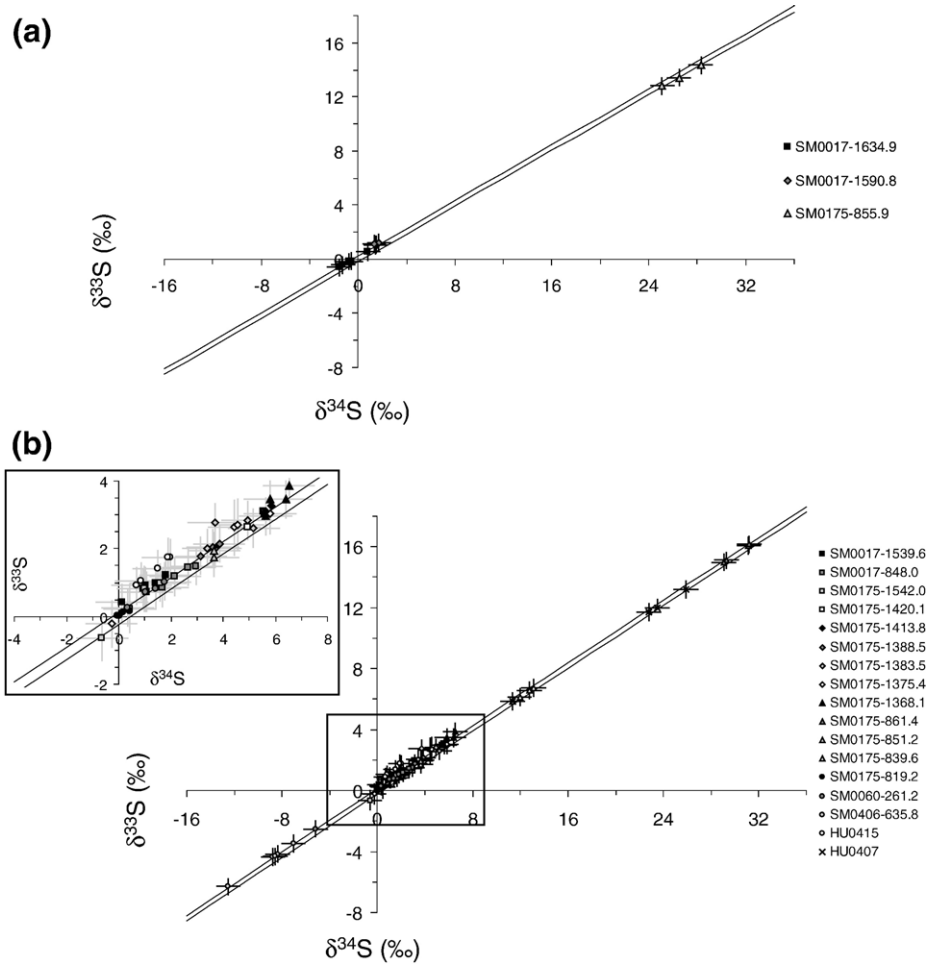

Fig. 3. Three isotope plots of the sulfur isotope ratios of Huronian sulfides with *Session 1* shown in (a) and *Session 2* along with inset in (b). The MDF bands calculated from the York regression are shown as 2σ deviations from the slope of 0.518. Error bars are 2σ and combine the internal and external errors.

5.2. Correlations of Huronian and Transvaal successions and the evolution of the sulfur cycle

Studies of sulfur isotope geochemistry in the Paleoproterozoic have so far revealed that significant (up to 35‰) fluctuations of $\delta^{34}S_{sulfide}$ values first occurred during the deposition of the Timeball Hill black shales in the Transvaal [6,52] and that these large variations continued after the period of cyclic glaciations [5,40]. This is shown in Fig. 5, where our new data are plotted with a compilation of published $\Delta^{33}S$ and $\delta^{34}S_{sulfide}$ values for Paleoproterozoic sedimentary rocks. The intercratonic correlation of glacial diamictites is complicated because of poor geochronological constraints and a limited number of studies of sulfur isotopes during glacial–interglacial intervals in the Paleoproterozoic. We note that the compilation in Fig. 5 is subjected to biases that stem from different interpretations of ages based on stratigraphic correlations and for the position of delta-values during interglacial periods. Most published data,

Fig. 4. Huronian sulfur chemostratigraphy showing new sulfur isotope data from sulfides in Huronian interglacial sediments. Parts (a) to (d) are for the analyzed portions of cores as shown in Fig. 1 (stratigraphic information was provided by the Ontario Ministry of Mines and Northern Developments), whereas (e) shows the integrated data. Pyrite (□), pyrrhotite (◇) and chalcopyrite (Δ) are plotted against Huronian formations and filled black symbols are for authigenic sulfides, those filled with gray represent sulfides interpreted to have an ambiguous origin and open symbols are for detrital sulfides. Error bars are 2σ and combine the internal and external errors. MIF sulfur isotopes in authigenic sulfides imply an anoxic atmosphere at the time of deposition, while the absence of MIF indicates O_2 concentrations >0.0002% only in authigenic sulfides.

including post-glaciation data plotted in Fig. 5, were assigned the median age between current age constraints for the host sedimentary rocks (error bars are not shown for simplicity). The demise of large magnitude MIF $\Delta^{33}S$ values is known to have occurred before or during the early Paleoproterozoic glaciations [2,5,6]. An important

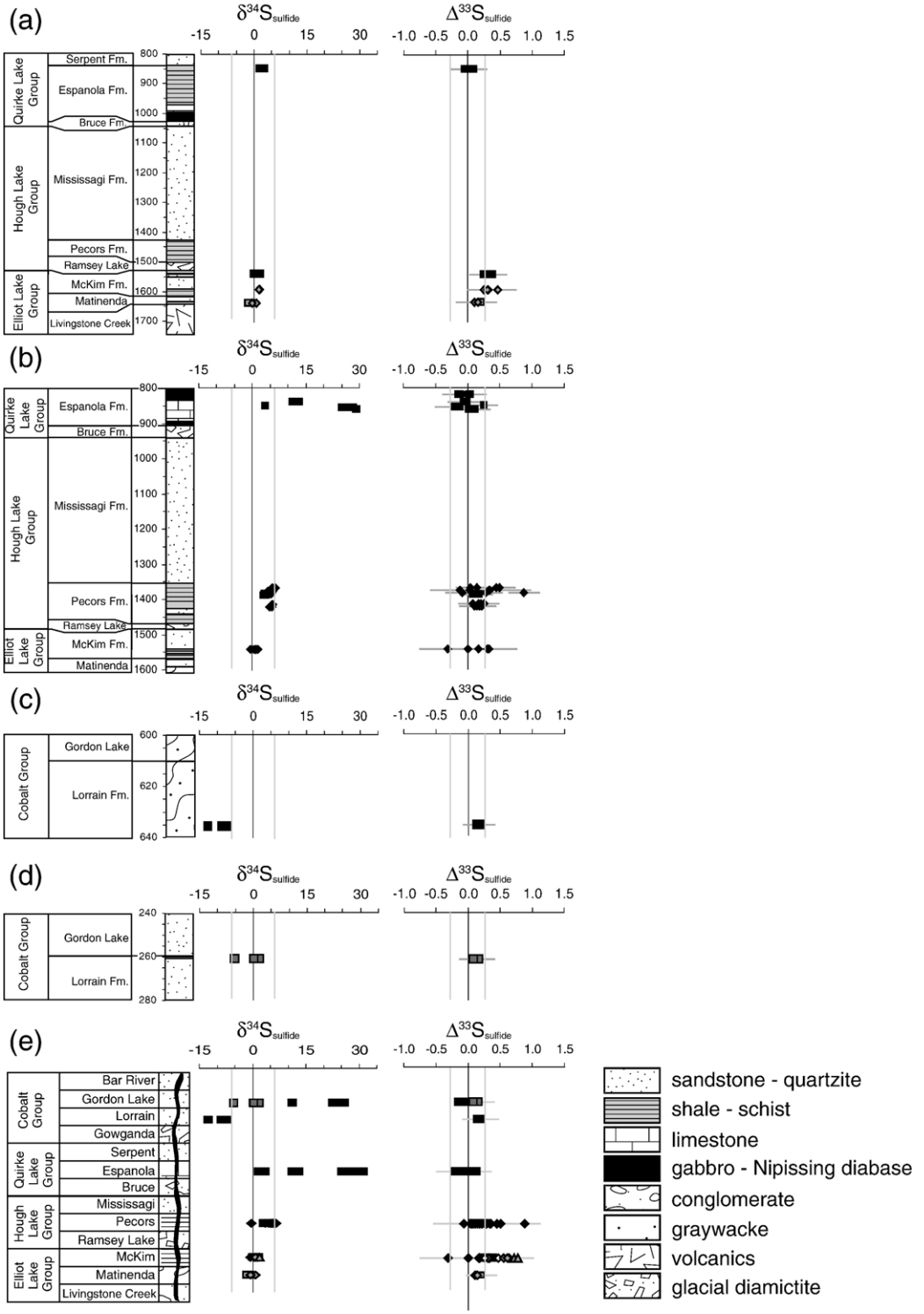

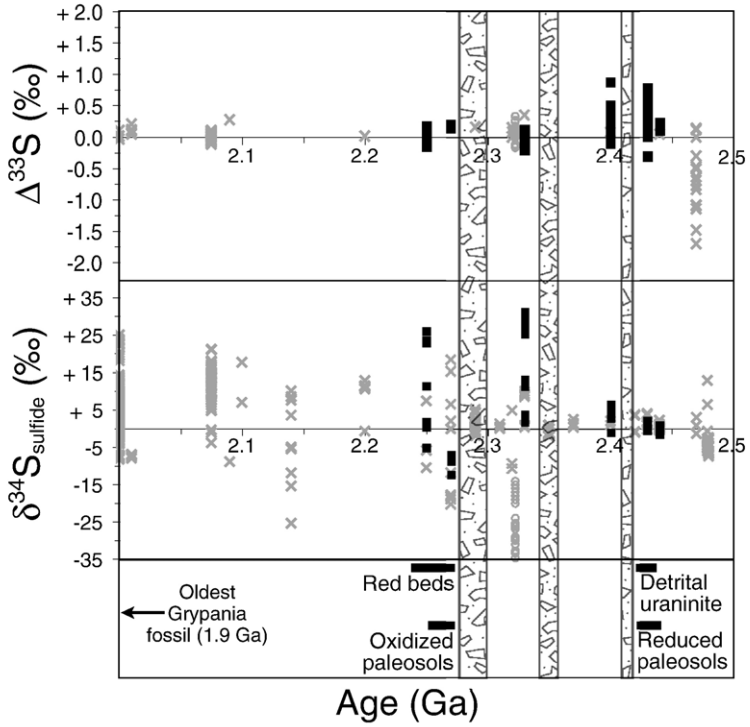

Fig. 5. New sulfur isotope data from Huronian sediments (■) plotted with published $\Delta^{33}S$ and $\delta^{34}S$ data for 2.0–2.5 Ga sediments (×). Note that all the new sulfur isotope data are shown (see text and Table 4 for interpretations of sulfide origins). The data for the Timeball Hill Fm. (○) are from Bekker et al. [6] and Cameron (1982) (references used for published data can be found in the supplementary data file). Ages for published isotope data are the median between the known age constraints. Ages estimated for the three glacial diamictites (labeled as in Fig. 4) are based on age constraints for the Huronian Supergroup, previously proposed correlations of Paleoproterozoic glacial diamictites, geochronological data from the Transvaal and chemostratigraphic global correlations of $\Delta^{33}S$ values (see also text). As described in the text, this correlation is possible but remains uncertain. The lower part of the figure shows approximate periods for some key indicators of atmospheric oxygenation in the Huronian and the oldest occurrence of Grypania.

observation that appears to be related to changes in sulfur cycling is that glacial diamictites in the Huronian Supergroup are coeval with diamictites in the Transvaal Supergroup, which are constrained by the 2.48 Ga Penge Iron Fm. (U–Pb on zircon; Trendall et al. cited in [53]), by an interglacial period at 2.32 Ga (Re–Os on pyrite; [54]) and by U–Pb analyses of zircons from the overlying 2.25 Ga Hekpoort and 2.22 Ga Ongeluk volcanics [55]. The correlation of individual diamictites from North America and South Africa is currently not further constrained by geochronology and various correlations have been proposed. For instance the diamictite in the lower Duitschland Fm. may be correlated with the Bruce diamictite [17,54,56], but it may also be contemporaneous with the Ramsey Lake diamictite. Furthermore, the other glacial diamictite in the Transvaal Supergroup is in the upper Timeball Hill/Boshoek Fm., which appears correlated with the Makganyene diamictite [54,56]. However on the basis of undocumented field observations of the contact between the Makganyene and Ongeluk Fm., this diamictite was also proposed to be younger than the Huronian glaciations [34,57]. This is significant because paleomagnetic data for the overlying Ongeluk lavas indicate that the Makganyene diamictite was deposited at latitudes within 11° of the equator, which may qualify the last Paleoproterozoic glaciation in North America as part of a "Snowball Earth" event [58]. However, paleomagnetic studies so far do not strongly support a low latitude paleogeography for the Superior Craton in the early Paleoproterozoic [34,35]. Because the younger age constraint for the Transvaal glaciations is identical to that of the Huronian, we argue that this proposed fourth Paleoproterozoic glaciation is unlikely. Single spot ion microprobe U–Pb analyses of detrital zircons in Transvaal sediments have revealed various zircon populations including one between ca. 2.45 and 2.20 Ga, which has been used to suggest a 200 Ma hiatus in deposition between the lower and upper parts of the Transvaal Supergroup [59]. The latter study has been used to argue that the Transvaal glaciations were not simultaneous with

the North American glaciations, but occurred shortly after. If larger numbers of Paleoproterozoic sedimentary rocks could be dated directly (e.g. by Re–Os), inter-cratonic correlations of sedimentary assemblages would provide additional support for the hypothesis that some of these glaciations were Paleoproterozoic Snowball Earth events. The apparently extensive glaciation in North America was proposed on the basis intra-cratonic correlations that link the Gowganda Fm. in the Huronian with the Headquarter Fm. (Snowy Pass), Enchantment Fm. (Marquette Range), Chibougamau Fm. (Mistassini) and Padlei Fm. (Hurwitz) [49]. We maintain that the extent of this glaciation is likely related to the last glaciation in the Transvaal, but so far this is not supported by further geochronological constraints.

A recent study of the organic geochemistry of the pre-glacial Matinenda Fm. has documented oil droplets with relatively high levels of 2α-methylhopanes and other biomarkers interpreted to be eukaryotic in origin [22]. It was also suggested that the oil probably migrated in the Matinenda Fm. from the McKim Fm. during post-depositional processes and consider unlikely the possibility that these cyanobacterial biomarkers are indigenous to the Matinenda Fm. Immediately before the first Huronian glaciation, only a few authigenic sulfides from McKim argillites have small magnitude MIF $\Delta^{33}S$ values, which can be interpreted to indicate low concentrations of atmospheric O_2 (<0.0002 vol.%) at the time of deposition. However, because these MIF deviations and ranges are small compared to some $\Delta^{33}S$ values in Archean sedimentary rocks, additional data at higher stratigraphic resolution are warranted to confirm this interpretation. Furthermore, published [2] and unpublished [41] sulfur isotope data for the McKim Fm. suggest very small magnitude MIF variations in these siliciclastic water-lain sediments (Table 5). Our data for sulfides of ambiguous origin from an amphibolite facies argillite from the McKim Fm. suggest that small MIF values may be preserved, but results underscore the need for additional analyses. Deep lacustrine or marine clays from the upper parts of the Pecors Fm., which overlie the Ramsey Lake diamictite, contain sulfides we interpreted to be authigenic with resolvable MIF $\Delta^{33}S$ deviations. The presence of small magnitude MIF signatures in these interglacial pelitic sedimentary rocks is significant because euhedral pyrites from the Espanola cap carbonate have unambiguous sedimentary sulfur with near-zero $\Delta^{33}S$ values (Table 5). Authigenic sulfides with small magnitude MIF signatures in the Pecors Fm. suggest low atmospheric O_2 levels in the time that followed the first Paleoproterozoic glaciation. The presence of such MIF $\Delta^{33}S$ values in Pecors sulfides suggest that the atmosphere was anoxic between the first and second glaciations and that the concentration of atmospheric O_2 increased beyond 0.0002 vol.%. [3] during this interval (Fig. 4). However, it is unclear if this signal represents a transient return to an anoxic atmosphere or if it indicates the terminus of the long-standing anoxic Archean surface zone. It is interesting to note the similarity between sulfide bands in the Pecors Fm. which display heterogeneous MIF values and sulfide bands in the ~2.63 Ga Jeerinah Fm. with $\Delta^{33}S$ values that vary between +0.2 and +0.8‰ within a few hundred microns [60].

In contrast to the MIF deviations recorded during the first interglacial period, authigenic pyrites from the Espanola Fm. have sulfur isotopes that suggest a more oxidized sulfur cycle with sufficient oxygen to inhibit or affect atmospheric photochemical reactions, and fluctuations in seawater $\delta^{34}S_{sulfate}$ and/or in sulfate concentrations. This could have occurred in response to more significant inputs of sulfate from crustal sulfide oxidation during episodes of global thawing, which perhaps also diluted MIF $\Delta^{33}S$ deviations in sulfate before MSR. The range of $\delta^{34}S_{sulfide}$ from Espanola carbonates is in excess of 30‰, which may indicate the activity of sulfate reduction by microbes. A single published $\delta^{34}S_{sulfate}$ value of +11.8‰ for Espanola carbonate-associated sulfate [11] is currently inadequate to assess if possible post-glacial variations in $\delta^{34}S_{sulfate}$ modulated the $\delta^{34}S_{pyrite}$ values, or if variable rates of MSR were synchronous with fluctuating concentration and/or inputs of dissolved sulfate to seawater. The large range of positive $\delta^{34}S_{pyrite}$ values in Espanola carbonate may be contemporaneous with the negative $\delta^{34}S_{pyrite}$ values from Timeball Hill black shales as suggested in Fig. 5. This attempted correlation could be supported (or refuted) by further multiple sulfur isotope analyses of authigenic sulfides from the Duitschland Fm., some of which may preserve small MIF $\Delta^{33}S$ deviations. During this near-synchronous interglacial period in the Transvaal Supergroup, evidence for MSR in high sulfate concentrations has been reported for the lower Timeball Hill Fm. [6,52] and carbonates from the upper Duitschland Fm. precipitated with high $\delta^{13}C_{carb}$ values [56,61].

As shown in Fig. 5, Huronian sulfides in post-Gowganda shallow marine sediments preserve evidence for fluctuating levels of seawater sulfate and/or $\delta^{34}S_{sulfate}$. For instance, sulfides in Lorrain argillites have $\delta^{34}S$ values between −12.5 and −7.1‰, which suggests MSR in non-limiting sulfate concentrations, whereas pyrites with a large range of $\delta^{34}S$ values between −5.2 and +25.9‰ from Gordon Lake red beds suggest relatively low seawater sulfate concentrations at the time of deposition as well as the activity of MSR. However, the occurrence of various sulfate phases in Gordon Lake sediments such as

anhydrite nodules with $\delta^{34}S$ values in excess of +15.6‰ [39] and barite with $\delta^{34}S$ values around +12.2‰ [62] suggests variable seawater sulfate concentrations and $\delta^{34}S_{sulfate}$. Combined with high $\delta^{34}S_{pyrite}$ values, the near-zero $\Delta^{33}S$ values for these pyrite grains indicate that atmospheric O_2 concentrations remained high after the Paleoproterozoic glaciations. Fluctuations in concentrations of seawater sulfate and/or in $\delta^{34}S_{sulfate}$ were proposed to explain the $\delta^{34}S_{sulfide}$ variations after the Paleoproterozoic glaciations. Based on this analysis, it now appears that the oxygenation of the early Paleoproterozoic atmosphere after the epoch of glaciations was an irreversible process [5].

5.3. Paleoproterozoic biogeochemical evolution

Links between the co-evolution of biogeochemical cycles with more active tectonic and magmatic processes during glacial–interglacial intervals in the early Paleoproterozoic have been proposed on the basis of carbon isotope data [63,64]. The tectonostratigraphic record of Late Archean and Paleoproterozoic sequences suggests that the Turee Creek glaciation (Western Australia) and the oldest Huronian glaciations occurred after a period of plume breakout and coincided with the assembly of a supercontinent [65]. Enhanced sedimentation and weathering rates during the breakup of a supercontinent in the early Paleoproterozoic could have been partly responsible for triggering the glaciation period by influencing the carbon–silicate cycles and resulted in a decrease of atmospheric CO_2. We propose that a consequence of these events was the increased delivery of nutrients such as dissolved phosphate to coastal waters, which is known to be a critical rate-limiting nutrient for oxygenic photosynthesis (e.g. [66]). An illustration of our model is shown in Fig. 6 where riverine input from weathering during rifting and glacial thawing leads to variations in seawater chemistry and translates to changes in microbial communities. Blooms of oxygenic photosynthesis could then have resulted in a decrease of atmospheric CH_4 levels and, along with lower CO_2 levels, led to perturbations in the greenhouse effect and to a colder climate. The Paleoproterozoic glacial–interglacial cycles could thus have been modulated by fluctuations in CH_4 and CO_2 as proposed in other studies [5,65,67].

Based on our results, we propose that atmospheric O_2 increased slightly before the first glaciation, and even more during the subsequent interglacial intervals. Thawing of large ice-sheets on Archean cratons during the early Paleoproterozoic must have resulted in higher erosion rates, denudation and runoff to increase delivery of phosphate to seawater. Recent studies have shown that phosphate levels were lowest in the Archean, and lower in the Paleoproterozoic, than at present [68]. Positive $\delta^{13}C_{carb}$ excursions in interglacial sedimentary rocks may point to higher burial rates of organic carbon [56], but higher rates of primary productivity worked hand-in-hand with these changes to the carbon cycle. If blooms of oxygenic photosynthesis were stimulated by phosphate delivery to seawater during interglacials, they would have gradually resulted in higher atmospheric O_2 levels (Fig. 6). Evidence for these blooms in Paleoproterozoic glacial periods may be uncovered by future carbon and nitrogen isotope studies, organic biomarker analyses and investigations of phosphate-rich sediments. Evidence for elevated primary productivity during Huronian interglacial periods is not present as $\delta^{13}C_{carb}$ excursions or as extensive stromatolite formations, but may be preserved in carbonates of the post-glacial Gordon Lake Fm. that contain high $\delta^{13}C$ values [62]. Finally, shales from the Pecors Fm. contain

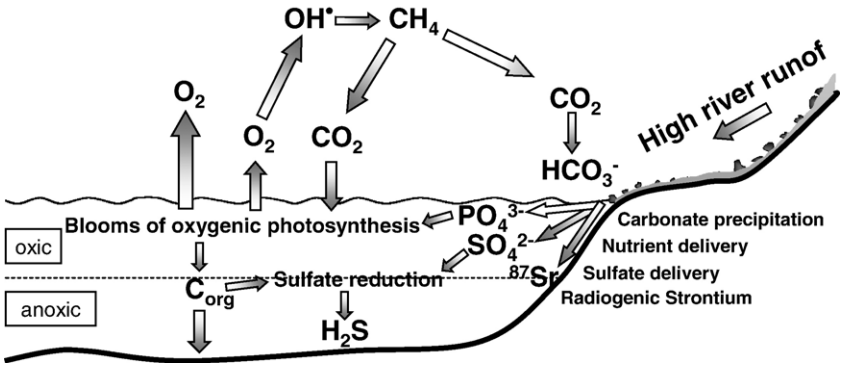

Fig. 6. Schematic illustration for our model of biogeochemical changes during interglacial periods in coastal seawater and in the atmosphere. This model is also proposed to have operated during the initial phase of rifting.

relatively low quantities of organic matter [81], but it is currently unclear if this was the result of post-glacial expansion of the biosphere.

By the end of the Huronian glacial period, levels of atmospheric O_2 and seawater SO_4^{2-} had increased in response to environmental changes. The three glacial cycles during the Early Paleoproterozoic were followed by a global $\delta^{13}C_{carb}$ excursion between ~2.25 and 2.05 Ga, interpreted to indicate elevated primary productivity and a significant accumulation of atmospheric O_2 [69]. The rise of O_2 concentration in the atmosphere of the post-glacial Paleoproterozoic Earth must have opened new ecological niches for aerobic micro-organisms. The discovery of mm-size fossils in the 1.9 Ga Marquette [70] and 1.7 Ga Changcheng (Northern China) [71] supergroups have been put forward as evidence that macroscopic eukaryotic life-forms emerged before the end of the Paleoproterozoic. Therefore we suggest that a new balance in the carbon cycle between oxygenic photosynthesizers and aerobic heterotrophs contributed to the end of the period of glacial–interglacial cycles.

Because similar perturbations of the carbon and sulfur cycles occurred in the Neoproterozoic, it may be informative to draw comparisons between the Paleoproterozoic and Neoproterozoic glacial–interglacial intervals. Neoproterozoic interglacial sediments deposited between two Snowball Earth events (Sturtian and Marinoan glaciations) have been found to have large range of positive $\delta^{34}S_{pyrite}$ values interpreted to represent biogeochemical changes in response to increased levels of O_2 [72,73]. If additional Paleoproterozoic interglacial sediments are found to preserve such high $\delta^{34}S_{pyrite}$ values, then it would be worthwhile to investigate whether this scenario for the Neoproterozoic is analogous. Some interglacial carbonates from Neoproterozoic successions preserve positive $\delta^{13}C_{carb}$ excursions [74,75], which may be similar to the Transvaal example of the Duitschland Fm. [56,61]. Our model for the causes of glaciations and atmospheric oxygenation is simple. Alternative models for the onset of global cooling and major glaciations have also been proposed including (1) an accumulation of continental crust at low latitude [76], (2) stratospheric dust from interstellar particles [77], and (3) a late origin of oxygenic photosynthesis that resulted in the destruction of a methane greenhouse [78]. Various models have also proposed different causes for atmospheric oxygenation in the Paleoproterozoic including: (1) atmospheric O_2 levels could not have risen until rates of oxygenic photosynthesis dominated over global oxygen sinks [65], (2) changes in the redox state of volcanic gases in the early Paleoproterozoic led to atmospheric oxygenation [79], (3) hydrodynamic escape of H_2 to space in the Archean could have gradually left residual O_2 in the atmosphere [80] and (4) the burial of organic carbon resulted in a net accumulation of atmospheric O_2 [69].

6. Conclusions

High-resolution ion microprobe analyses of sulfides from water-lain Huronian sedimentary rocks were performed in their petrographic context. Our analyses show that the assessment of sulfide authigenecity in Paleoproterozoic sedimentary rocks can be ambiguous, but helpful criteria such as sulfide chemistry, host lithology, mode of occurrence and isotopic composition can be used to distinguish authigenic from detrital sulfides. Ion microprobe analyses allow evaluation of these criteria that help in the interpretation of authigenecity. We found that only a small proportion of authigenic sulfides from the McKim and Pecors formations have small magnitude MIF $\Delta^{33}S$ values (<0.88‰). In contrast, authigenic sulfides from the Espanola and Gordon Lake formations have a large range of MDF $\delta^{34}S$ values. We interpret our new sulfur isotope data to indicate that an irreversible increase of atmospheric O_2 levels occurred between the first and second Huronian glaciations. We propose a model where enhanced weathering rates during interglacial thawing led to an elevated supply of nutrients (e.g. phosphate) in the oceans, which stimulated blooms of oxygenic photosynthesis. Global increases in rates of oxygenic photosynthesis likely played a crucial role in the accumulation of atmospheric O_2, and may have been related to changes in atmospheric CO_2 and CH_4 levels that possibly triggered subsequent Paleoproterozoic glaciations. The large ranges of ^{34}S-enriched authigenic sulfides in the Espanola cap carbonate and in post-Snowball Earth sediments from the Gordon Lake Fm suggest the activity of MSR in variable seawater sulfate concentrations, but may also reflect variations in $\delta^{34}S_{sulfate}$. It appears that atmospheric O_2 concentrations remained in excess of 0.0002 vol.% after the second Paleoproterozoic glaciation, and remained so beyond the glaciation period. At earlier times oxygenation events such as these would have been transitory, prevented either by the oxidation of reduced cations in the upper oceans or reduced gases in the atmosphere, or both. Our model of Paleoproterozoic events thus relates multiple geological and geochemical observations and includes testable predictions that will be the focus of future work.

Acknowledgments

We thank P. Boni for help in sample preparation and J. Drexler with assistance with the electron microprobe; M.

Hailstone (with special thanks to the Ontario Ministry of Northern Development and Mines) and K. Hattori for crucial help in sample acquisition; K. McKeegan, G. Jarzebinski and N. Cates for assistance with ion microprobe analyses; and A. Bekker, H. Elderfield, J. Farquhar, L. Kah, J. Kasting, L. Kump, J. Walker and B. Wing for discussions and comments that greatly improved the manuscript. Research support by the NASA Astrobiology Institute (NAI) to the CU Center for Astrobiology (S.J.M.) is gratefully appreciated. The UCLA ion microprobe laboratory is supported by the NSF Instrumentation and Facilities Program. The Fonds pour la recherche sur la nature et les technologies du Québec and an NAI graduate research grant to DP helped make this work possible.

Appendix A. Supplementary data

Supplementary data associated with this article can be found, in the online version, at doi:10.1016/j.epsl.2006.12.015.

References

[1] H.D. Holland, The chemical evolution of the atmosphere and oceans, Princeton Univ. Press, Princeton, 1984.
[2] J. Farquhar, H.M. Bao, M. Thiemens, Atmospheric influence of Earth's earliest sulfur cycle, Science 289 (2000) 756–758.
[3] A.A. Pavlov, J.F. Kasting, Mass-independent fractionation of sulfur isotopes in Archean sediments: strong evidence for an anoxic Archean atmosphere, Astrobiology 2 (2002) 27–41.
[4] J. Farquhar, J. Savarino, S. Airieau, M.H. Thiemens, Observation of wavelength-sensitive mass-independent sulfur isotope effects during SO_2 photolysis: implications for the early atmosphere, J. Geophys. Res. 106 (2001) 32829–32839.
[5] D. Papineau, S.J. Mojzsis, C.D. Coath, J.A. Karhu, K.D. McKeegan, Multiple sulfur isotopes of sulfides from sediments in the aftermath of Paleoproterozoic glaciations, Geochim. Cosmochim. Acta 69 (2005) 5033–5060.
[6] A. Bekker, H.D. Holland, P.L. Wang, D. Rumble, H.J. Stein, J.L. Hannah, L.L. Coetzee, N.J. Beukes, Dating the rise of atmospheric oxygen, Nature 427 (2004) 117–120.
[7] S.J. Mojzsis, C.D. Coath, J.P. Greenwood, K.D. McKeegan, T.M. Harrison, Mass-independent isotope effects in Archean (2.5 to 3.8 Ga) sedimentary sulfides determined by ion microprobe analysis, Geochim. Cosmochim. Acta 67 (2003) 1635–1658.
[8] D.E. Canfield, R. Raiswell, The evolution of the sulfur cycle, Am. J. Sci. 299 (1999) 697–723.
[9] K.S. Habicht, M. Gade, B. Thamdrup, P. Berg, D.E. Canfield, Calibration of sulfate levels in the Archean ocean, Science 298 (2002) 2372–2374.
[10] Y. Shen, R. Buick, D.E. Canfield, Isotopic evidence for microbial sulphate reduction in the early Archaean era, Nature 410 (2001) 77–81.
[11] D.J. Bottomley, J. Veizer, H. Nielsen, M. Moczydlowska, Isotopic composition of disseminated sulfur in Precambrian sedimentary rocks, Geochim. Cosmochim. Acta 56 (1992) 3311–3322.
[12] T.E. Krogh, D.W. Davis, F. Corfu, Precise U–Pb zircon and baddeleyite ages for the Sudbury area, in: E.G. Pye, A.J. Naldrett, P.E. Gilblin (Eds.), The geology and ore deposits of the Sudbury structure, Ontario Geol. Surv. Sp. Pap., vol. 1, 1984, pp. 431–446.
[13] F. Corfu, A.J. Andrews, A U–Pb age for mineralized Nipissing diabase, Gowganda, Ontario, Can. J. Earth Sci. 23 (1986) 107–109.
[14] S.M. Roscoe, K.D. Card, The reappearance of the Huronian in Wyoming: rifting and drifting of ancient continents, Can. J. Earth Sci. 30 (1993) 2475–2480.
[15] G.M. Young, D.G.F. Long, C.M. Fedo, H.W. Nesbitt, Paleoproterozoic Huronian basin: product of a Wilson cycle punctuated by glaciations and a meteorite impact, Sediment. Geol. 141–142 (2001) 233–254.
[16] G.M. Young, H.W. Nesbitt, The Gowganda Formation in the southern part of the Huronian outcrop Belt, Ontario, Canada: stratigraphy, depositional environments and regional tectonic significance, Precambrian Res. 29 (1985) 265–301.
[17] A. Bekker, A.J. Kaufman, J.A. Karhu, K.A. Eriksson, Evidence for Paleoproterozoic cap carbonates in North America, Precambrian Res. 137 (2005) 167–206.
[18] S. Roscoe, Huronian rocks and uraniferous conglomerates, Geol. Surv. Can. Pap. 68–40 (1969) 205.
[19] G.M. Young, Tectono-sedimentary history of Early Proterozoic rocks of the northern Great Lakes region, in: L.G. Medaris Jr (Ed.), Early Proterozoic geology of the Great Lakes region, Memoir, 160, The Geological Society of America, Boulder, 1983, pp. 15–32.
[20] A.I. Zolnai, R.A. Price, H. Helmstaedt, Regional cross section of the Southern Province adjacent to Lake Huron, Ontario: implications for the tectonic significance of the Murray Fault Zone, Can. J. Earth Sci. 21 (1984) 447–456.
[21] N. Prasad, S.M. Roscoe, Evidence of anoxic to oxic atmospheric change during 2.45–2.22 Ga lower and upper sub-Huronian paleosols, Canada, Catena 27 (1996) 105–121.
[22] A. Dutkiewicz, H. Volk, S.C. George, J. Ridley, R. Buick, Biomarkers from Huronian oil-bearing fluid inclusions: an uncontaminated record of life before the Great Oxidation Event, Geology 34 (2006) 437–440.
[23] A. Dutkiewicz, J. Ridley, R. Buick, Oil-bearing CO_2–CH_4–H_2O fluid inclusions: oil survival since the Palaeoproterozoic after high temperature entrapment, Chem. Geol. 194 (2003) 51–79.
[24] T.O. Willingham, N. Bartholomew, L.A. Nagy, D.H. Krinsley, D.J. Mossman, Uranium-bearing stratiform organic matter in paleoplacers of the lower Huronian Supergroup, Elliot Lake — Blind River region, Canada, Can. J. Earth Sci. 22 (1985) 1930–1944.
[25] P.W. Fralick, A.D. Miall, Sedimentology of the Lower Huronian Supergroup (Early Proterozoic), Elliot Lake area, Ontario, Canada, Sediment. Geol. 63 (1989) 127–153.
[26] G.M. Young, Diamictites of the Early Proterozoic Ramsey Lake and Bruce Formation, north shore of Lake Huron, Ontario, Canada, in: M.J. Hambrey, W.B. Harland (Eds.), Earth's pre-Pleistocene glacial record, Cambridge University Press, 1981, pp. 813–816.
[27] J. Veizer, R.W. Clayton, R.W. Hinton, Geochemistry of Precambrian carbonates: IV. Early Paleoproterozoic (2.25±0.25 Ga) seawater, Geochim. Cosmochim. Acta 56 (1992) 875–885.
[28] G.M. Young, Origin of carbonate-rich Early Proterozoic Espanola Formation, Ontario, Canada, Geol. Soc. Amer. Bull. 84 (1973) 135–160.
[29] L. Bernstein, G.M. Young, Depositional environments of the Early Proterozoic Espanola Formation, Ontario, Canada, Can. J. Earth Sci. 27 (1990) 539–551.

[30] H.J. Hofmann, D.A.B. Pearson, B.H. Wilson, Stromatolites and fenestral fabric in Early Proterozoic Huronian Supergroup, Ontario, Can. J. Earth Sci. 17 (1980) 1351–1357.
[31] G.M. Young, Proterozoic plate tectonic, glaciation and iron-formations, Sediment. Geol. 58 (1988) 127–144.
[32] F.W. Chandler, Sedimentology and paleoclimatology of the Huronian (Early Aphebian) Lorrain and Gordon Lake Formations and their bearing on models for sedimentary copper mineralization, Geol. Surv. Can. Pap. 86-1A (1986) 121–132.
[33] G.M. Young, Tillites and aluminous quartzites as possible time markers for middle Precambrian (Aphebian) rocks of North America, in: G.M. Young (Ed.), Huronian stratigraphy and sedimentation, Special Paper 12, Geological Association of Canada, 1973, pp. 97–127.
[34] I.A. Hilburn, J.L. Kirschvink, E. Tajika, R. Tada, Y. Hamano, S. Yamamoto, A negative fold test on the Lorrain Formation of the Huronian Supergroup: uncertainty on the paleolatitude of the Paleoproterozoic Gowganda glaciation and implications for the great oxygenation event, Earth Planet. Sci. Lett. 232 (2005) 315–332.
[35] G.E. Williams, P.W. Schmidt, Paleomagnetism of the Paleoproterozoic Gowganda and Lorrain formations, Ontario: low paleolatitude for Huronian glaciations, Earth Planet. Sci. Lett. 153 (1997) 157–169.
[36] F.W. Chandler, Sedimentary setting of an Early Proterozoic copper occurrence in the Cobalt Group, Ontario: a preliminary assessment, Geol. Surv. Can. Pap. 84-1A (1984) 185–192.
[37] F.W. Chandler, Diagenesis of Sabkha-related, sulphate nodules in the Early Proterozoic Grodon Lake Formation, Ontario, Canada, Carbonate Evaporite 3 (1988) 75–94.
[38] C.M. Fedo, G.M. Young, H.W. Nesbitt, J.M. Hanchar, Potassic and sodic metasomatism in the Southern Province of the Canadian Shield: evidence from the Paleoproterozoic Serpent Formation, Huronian Supergroup, Canada, Precambrian Res. 84 (1997) 17–36.
[39] E.M. Cameron, Evidence from Early Proterozoic anhydrite for sulphur isotopic partitioning in Precambrian oceans, Nature 304 (1983) 54–56.
[40] K. Hattori, H.R. Krouse, F.A. Campbell, The start of sulfur oxidation in continental environments — about 2.2×10^9 years ago, Science 221 (1983) 549–551.
[41] B.A. Wing, E. Brabson, J. Farquhar, A.J. Kaufman, D. Rumble, A. Bekker, $\Delta^{33}S$, $\delta^{34}S$ and $\delta^{13}C$ constraints on the Paleoproterozoic atmosphere during the earliest Huronian glaciation, Geochim. Cosmochim. Acta A66 (2002) A840.
[42] S. Tachibana, T. Hirai, K. Goto, S. Yamamoto, Y. Isozaki, R. Tada, E. Tajika, G. Shimoda, Y. Morishita, N.T. Kita, Sulfur isotopic composition of sulfides from the lower Huronian Supergroup, Ontario, Canada, Eos, Trans. - Am. Geophys. Union 85 (2004) (abstract).
[43] H. Ohmoto, M.B. Goldhaber, Sulfur and carbon isotopes, in: H.L. Barnes (Ed.), Geochemistry of hydrothermal ore deposits, John Wiley and Sons, New York, 1997.
[44] W.A. Russell, D.A. Papanastassiou, T.A. Tombrello, Ca isotope fractionation on the Earth and other solar system materials, Geochim. Cosmochim. Acta 42 (1978) 1075–1090.
[45] K.I. Mahon, The new "York" regression: application of an improved statistical method to geochemistry, Int. Geol. Rev. 38 (1996) 293–303.
[46] J. Farquhar, D.T. Johnston, B.A. Wing, K.S. Habicht, D.E. Canfield, S. Airieau, M.H. Thiemens, Multiple sulphur isotopic interpretations of biosynthetic pathways: implications for biological signatures in the sulphur isotope record, Geobiology 1 (2003) 27–36.
[47] J. Farquhar, B.A. Wing, Multiple sulfur isotopes and the evolution of the atmosphere, Earth Planet. Sci. Lett. 213 (2003) 1–13.
[48] S. Ono, B. Wing, D. Rumble, J. Farquhar, High precision analysis of all four stable isotopes of sulfur (S-32, S-33, S-34 and S-36) at nanomole levels using a laser fluorination isotope-ratio-monitoring gas chromatography–mass spectrometry, Chem. Geol. 225 (2006) 30–39.
[49] R.W. Ojakangas, Glaciation: an uncommon "mega-event" as a key to intracontinental and intercontinental correlation of Early Proterozoic basin fill, North American and Baltic cratons, in: K. L. Kleinspehn, C. Paola (Eds.), New perspectives in basin analysis, Springer-Verlag, New York, 1988, pp. 431–444.
[50] S. Ono, B. Wing, D. Johnston, J. Farquhar, D. Rumble, Mass-dependent fractionation of quadruple stable sulfur isotope system as a new tracer of sulfur biogeochemical cycles, Geochim. Cosmochim. Acta 70 (2006) 2238–2252.
[51] D. Johnston, B. Wing, J. Farquhar, A.J. Kaufman, H. Strauss, T.W. Lyons, L.C. Kah, D.E. Canfield, Active microbial sulfur disproportionation in the Mesoproterozoic, Science 310 (2005) 1477–1479.
[52] E.M. Cameron, Sulphate and sulphate reduction in early Precambrian oceans, Nature 296 (1982) 145–148.
[53] D.R. Nelson, A.F. Trendall, W. Altermann, Chronological correlations between the Pilbara and Kaapvaal cratons, Precambrian Res. 97 (1999) 165–189.
[54] J.L. Hannah, A. Bekker, H.J. Stein, R.J. Markey, H.D. Holland, Primitive Os and 2316 Ma age for marine shale: implications for Paleoproterozoic glacial events and the rise of atmospheric oxygen, Earth Planet. Sci. Lett. 225 (2004) 43–52.
[55] H. Dorlan, Provenance, ages, and timing of sedimentation of selected Neoarchean and Paleoproterozoic successions on the Kaapvaal craton, Ph.D. thesis, Rand Afrikaans University, 2004.
[56] A. Bekker, A.J. Kaufman, J.A. Karhu, N.J. Beukes, Q.D. Swart, L.L. Coetzee, K.A. Eriksson, Chemostratigraphy of the Paleoproterozoic Duitschland Formation, South Africa: implications for coupled climate change and carbon cycling, Am. J. Sci. 301 (2001) 261–285.
[57] R.E. Kopp, J.L. Kirschvink, I.A. Hilburn, C.Z. Nash, The Paleoproterozoic snowball Earth: a climate disaster triggered by the evolution of oxygenic photosynthesis, Proceeding of the National Academy of Science of the United States of America, vol. 102, 2005, pp. 11131–11136.
[58] D.A. Evans, N.J. Beukes, J.L. Kirschvink, Low-latitude glaciation in the Palaeoproterozoic era, Nature 386 (1997) 262–266.
[59] R.B.M. Mapeo, R.A. Armstrong, A.B. Kampunzu, M.P. Modisi, L.V. Ramokate, B.N.J. Modie, A ca. 200 Ma hiatus between the Lower and Upper Transvaal Groups of southern Africa: SHRIMP U–Pb detrital zircon evidence from the Segwagwa Group, Botswana: implications for Palaeoproterozoic glaciations, Earth Planet. Sci. Lett. 244 (2006) 113–132.
[60] S. Ono, B.A. Wing, D. Rumble, J. Farquhar, High precision analysis of all four stable isotopes of sulfur (^{32}S, ^{33}S, ^{34}S and ^{36}S) at nanomole levels using a laser fluorination isotope-ratio-monitoring gas chromatography–mass spectrometry, Chem. Geol. 225 (2006) 30–39.
[61] I.S. Buick, R. Uken, R.L. Gibson, T. Wallmach, High-$\delta^{13}C$ Paleoproterozoic carbonates from the Transvaal Supergroup, South Africa, Geology 26 (1998) 875–878.

[62] A. Bekker, J.A. Karhu, A.J. Kaufman, Carbon isotope record for the onset of the Lomagundi carbon isotope excursion in the Great Lakes area, North America, Precambrian Res. 148 (2006) 145–180.
[63] J.F. Lindsay, M.D. Brasier, Did global tectonics drive early biosphere evolution? Carbon isotope record from 2.6 to 1.9 Ga carbonates of Western Australian basins, Precambrian Res. 114 (2002) 1–34.
[64] A. Bekker, J.A. Karhu, K.A. Eriksson, A.J. Kaufman, Chemostratigraphy of Paleoproterozoic carbonate successions of the Wyoming Craton: tectonic forcing of biogeochemical change? Precambrian Res. 120 (2003) 279–325.
[65] M.E. Barley, A. Bekker, B. Krapez, Late Archean to Early Paleoproterozoic global tectonics, environmental change and the rise of atmospheric oxygen, Earth Planet. Sci. Lett. 238 (2005) 156–171.
[66] K. Fennel, M. Follows, P.G. Falkowski, The co-evolution of the nitrogen, carbon and oxygen cycles in the Proterozoic ocean, Am. J. Sci. 305 (2005) 526–545.
[67] J.F. Kasting, Methane and climate during the Precambrian era, Precambrian Res. 137 (2005) 119–129.
[68] C.J. Bjerrum, D.E. Canfield, Ocean productivity before about 1.9 Gyr ago limited by phosphorous adsorption onto iron oxides, Nature 417 (2002) 159–162.
[69] J.A. Karhu, H.D. Holland, Carbon isotopes and the rise of atmospheric oxygen, Geology 24 (1996) 867–870.
[70] T.M. Han, B. Runnegar, Megascopic eukaryotic algae from the 2.1-billion-year-old Negaunee iron-formation, Michigan, Science 257 (1992) 232–235.
[71] S.X. Zhu, H.N. Chen, Megascopic multicellular organisms from the 1700-million-year-old Tuanshanzi Formation in the Jixian area, North China, Science 270 (1995) 620–622.
[72] P. Gorjan, J.J. Veevers, M.R. Walter, Neoproterozoic sulfur-isotope variation in Australia and global implications, Precambrian Res. 100 (2000) 151–179.
[73] M.T. Hurtgen, M.A. Arthur, G.P. Halverson, Neoproterozoic sulfur isotopes, the evolution of microbial sulfur species, and the burial efficiency of sulfide as sedimentary pyrite, Geology 33 (2005) 41–44.
[74] P.F. Hoffman, D.P. Schrag, The snowball Earth hypothesis: testing the limits of global change, Terra Nova 14 (2002) 129–155.
[75] A.J. Kaufman, Neoproterozoic variations in the C-isotopic composition of seawater — stratigraphic and biogeochemical implications, Precambrian Res. 73 (1995) 27–49.
[76] D.P. Schrag, R.A. Berner, P.F. Hoffman, G.P. Halverson, On the initiation of a snowball Earth, Geochem. Geophys. Geosyst. 3 (2002) U1–U21.
[77] A.A. Pavlov, O.B. Toon, A.K. Pavlov, J. Bally, D. Pollard, Passing through a giant molecular cloud: "Snowball" glaciations produced by interstellar dust — art. no. L03705, Geophys. Res. Lett. 32 (2005) 3705–3705.
[78] R.E. Kopp, J.L. Kirschvink, I.A. Hilburn, C.Z. Nash, The paleoproterozoic snowball Earth: a climate disaster triggered by the evolution of oxygenic photosynthesis, Proc. Natl. Acad. Sci. U. S. A. 102 (2005) 11131–11136.
[79] L.R. Kump, J.F. Kasting, M.E. Barley, Rise of atmospheric oxygen and the "upside-down" Archean mantle, Geochem. Geophys. Geosyst. 2 (2001) U1–U10.
[80] D.C. Catling, K.J. Zahnle, C.P. McKay, Biogenic methane, hydrogen escape, and the irreversible oxidation of early Earth, Science 293 (2001) 839–843.
[81] A.J. Kaufman, A. Bekker, Sedimentary and isotopic characterization of the Paleoproterozoic glacial interval, Geol. Soc. Amer. Abstracts with Programs 36 (2004) 341.